City Research Online

City, University of London Institutional Repository

Citation: Bianchi, L., Forini, V., Leder, B., Töpfer, P. & Vescovi, E. (2020). New linearization and reweighting for simulations of string sigma-model on the lattice. The Journal of High Energy Physics, 2020(1), 174. doi: 10.1007/jhep01(2020)174

This is the accepted version of the paper.

This version of the publication may differ from the final published version.

Permanent repository link: https://openaccess.city.ac.uk/id/eprint/23722/

Link to published version: https://doi.org/10.1007/jhep01(2020)174

Copyright: City Research Online aims to make research outputs of City, University of London available to a wider audience. Copyright and Moral Rights remain with the author(s) and/or copyright holders. URLs from City Research Online may be freely distributed and linked to.

Reuse: Copies of full items can be used for personal research or study, educational, or not-for-profit purposes without prior permission or charge. Provided that the authors, title and full bibliographic details are credited, a hyperlink and/or URL is given for the original metadata page and the content is not changed in any way.

City Research Online: http://openaccess.city.ac.uk/ publications@city.ac.uk

Published for SISSA by Springer

Received: October 24, 2019
Revised: January 4, 2020
Accepted: January 17, 2020
Published: January 28, 2020

New linearization and reweighting for simulations of string sigma-model on the lattice

L. Bianchi,[a] **V. Forini,**[b,c] **B. Leder,**[c] **P. Töpfer**[c] **and E. Vescovi**[e]

[a] *Centre for Research in String Theory, Queen Mary University of London, Mile End Road, London E1 4NS, U.K.*
[b] *Department of Mathematics, City, University of London, Northampton Square, EC1V 0HB London, U.K.*
[c] *Institut für Physik, Humboldt-Universität zu Berlin and IRIS Adlershof, Zum Großen Windkanal 6, 12489 Berlin, Germany*
[e] *The Blackett Laboratory, Imperial College, London SW7 2AZ, U.K.*

E-mail: lorenzo.bianchi@qmul.ac.uk, valentina.forini@city.ac.uk, leder@physik.hu-berlin.de, philipp.toepfer@physik.hu-berlin.de, e.vescovi@imperial.ac.uk

Abstract: We study the discretized worldsheet of Type IIB strings in the Gubser-Klebanov-Polyakov background in a new setup, which eliminates a complex phase previously detected in the fermionic determinant. A sign ambiguity remains, which a study of the fermionic spectrum shows to be related to Yukawa-like terms, including those present in the original Lagrangian before the linearization standard in a lattice QFT approach. Monte Carlo simulations are performed in a large region of the parameter space, where the sign problem starts becoming severe and instabilities appear due to the zero eigenvalues of the fermionic operator. To face these problems, simulations are conducted using the absolute value of a fermionic Pfaffian obtained introducing a small twisted-mass term, acting as an infrared regulator, into the action. The sign of the Pfaffian and the low modes of the quadratic fermionic operator are then taken into account by a reweighting procedure of which we discuss the impact on the measurement of the observables. In this setup we study bosonic and fermionic correlators and observe a divergence in the latter, which we argue — also via a one-loop analysis in lattice perturbation theory — to originate from the U(1)-breaking of our Wilson-like discretization for the fermionic sector.

Keywords: AdS-CFT Correspondence, Integrable Field Theories, Lattice Quantum Field Theory, Wilson, 't Hooft and Polyakov loops

ArXiv ePrint: 1910.06912

Open Access, © The Authors.
Article funded by SCOAP[3].

https://doi.org/10.1007/JHEP01(2020)174

Contents

1 Introduction and discussion **1**

2 Linearization and phase-free Pfaffian **4**

3 Spectrum of the fermionic operator **7**

4 Simulations at finite coupling **9**
4.1 Observables 10
4.1.1 The $\langle xx^* \rangle$ correlator 10
4.1.2 The fermionic correlators 13
4.2 Impact of reweighting on observables 17

A Conventions and matrix algebra **21**

B One-point function for x, x^* **23**

JHEP01(2020)174

1 Introduction and discussion

Lattice field theory methods are already employed for some time in the broad context of AdS/CFT (see e.g. [1–9]), and more recently also from the point of view of string sigma-models in AdS backgrounds [10–14]. In this case the focus has been on a particularly central model for the AdS/CFT community, the string worldsheet dual to a light-like cusped Wilson loop. The renormalization of the latter is governed by the cusp anomalous dimension, an observable of crucial importance in all gauge theories and also in the maximally supersymmetric one, $\mathcal{N} = 4$ super Yang-Mills in four dimensions. Its non-perturbative behavior is there accessible exactly, when using the assumption and the tools of integrability [15–19]. From the perspective of superstring theory, the relevant sigma-model — a Green-Schwarz action in $AdS_5 \times S^5$ background with Ramond-Ramond flux — is a complicated, highly non-linear two-dimensional field theory which is not known how to solve exactly and has been approached perturbatively, so far up to two-loop level, in a semiclassical way. Applying lattice field theory methods for its non-perturbative investigation appears to be a formidable benchmark test for a wider program which aims at using this approach to numerical holography in much more general cases, for which exact predictions do not exist. This is particularly true since, as from the preliminary results of ref. [12], this model appears to present in a single setup many of the challenges of lattice investigations in QFT, such as e.g. symmetry-breaking discretizations, numerical instabilities and even a complex phase problem. In this paper we make significant steps in addressing these points.

The model under study is the AdS-lightcone gauge-fixed, Type IIB Green-Schwarz superstring action [20, 21] describing fluctuations about the Gubser-Klebanov-Polyakov

background [22], and was worked out explicitly in [23]. From the point of view of an investigation with lattice field theory methods, it is a non-linear action with no gauge degrees of freedom and where fermions, which couple via a quartic interaction, do not carry (Lorentz) spinor indices but are just a set of anticommuting scalars. A global $\mathrm{SO}(6)\times\mathrm{SO}(2)$ symmetry is explicitly realized. In continuum perturbation theory, results are available up to two loop order [23, 24] (see also [25]).

The analysis of refs. [11, 12] presented a discretization of the (linearized) model based on a Wilson-like treatment of the fermionic sector which was tested via a one-loop analysis in lattice perturbation theory. An estimation of the (derivative) of the cusp anomaly of $\mathcal{N}=4$ super Yang-Mills was provided, via a measurement of the vacuum expectation value of the relevant action in terms of simulations performed employing a Rational Hybrid Monte Carlo (RHMC) algorithm. In this context, the (dimensionless) coupling constant is the effective string tension $g=\frac{R^2}{4\pi\alpha'}\equiv\frac{\sqrt{\lambda}}{4\pi}$, where R is the common radius of AdS_5 and S^5 and λ is the 't Hooft coupling, and the perturbative expansion is a series in inverse powers of the effective string tension. Therefore, the string sigma-model is weakly coupled for large values of g and in this regime, a good qualitative agreement was observed with the exact predictions obtained via integrability methods. In the case of higher-order fermionic interactions, one proceeds first linearizing the model via the introduction a set of auxiliary fields, then integrates out the fermionic determinant/Pfaffian re-exponentiating it in terms of a set of bosonic fields called pseudio-fermions and letting it become part of the Boltzmann weight of configurations in the statistical ensemble. It was observed in [12] that the nature of the quartic interaction — in which a "repulsive" potential appears — is responsible for the appearance of a non-hermitian piece in the linearized Lagrangian, which eventually gives rise to a *complex phase* in the fermionic Pfaffian. For lower values of g, namely when the string sigma-model is strongly coupled, a severe sign problems appears.

In what follows we discuss a new linearization of the four-fermion term[1] which eliminates the complex phase — albeit not the sign problem (this is expected in most systems with interacting fermions). We will proceed via an algebraic manipulation of the original fermionic Lagrangian. The resulting quadratic fermionic operator O_F is antisymmetric and "γ_5-hermitian", two properties which ensure a real, non-negative $\det O_F$ and a *real* Pfaffian $(\mathrm{Pf}\, O_F)^2=\det O_F\geq 0$. This is quite crucial, as eliminating the complex phase allows to eliminate a systematic error in measurements, in particular in the so-called reweighting procedure (see section 4 below), in which the possibly present phase would have to be calculated explicitly.[2] Because of the sign ambiguity in $\mathrm{Pf}\, O_F=\pm\sqrt{\det O_F}$, a sign problem may still remain, which is in fact the case. Below — via a study of the fermionic spectrum [13] — we show that the sign ambiguity appears to be related to the Yukawa-like terms, including those present before linearization, and therefore in the original Lagrangian. By looking at the lowest eigenvalue for the squared fermionic operator $\hat{O}_F^\dagger\hat{O}_F$ in a large region

[1] This new linearization has been presented at various conferences and in the proceedings [13].

[2] An efficient evaluation of complex determinants for arbitrarily large matrices is highly non trivial. For this reason, in [12] this has been done only for small lattices. It was there observed that the reweighting had no effect on the central value of the observables under study, therefore the phase was omitted from the simulations when taking the continuum limit ($N\to\infty$). In absence of data for larger lattices the possible systematic error related to this procedure was not assessed.

JHEP01(2020)174

of the parameter space, we also observe below that sign flips are extremely unlikely in an interesting regime of the coupling, $g \simeq 10$.

Together with the sign problem, for lower values of g the zero eigenvalues of the fermionic operator cause numerical instabilities, due to the non-convergence of the inverter for the fermionic matrix. Mimicking the twisted-mass reweighting procedure of [26] we perform simulations using the absolute value of a fermionic Pfaffian modified with an infrared regulator. The sign of the Pfaffian and the low modes of O_F are then taken into account by a reweighting procedure of which we discuss in details the impact on the measurement of the observables. We are confident that simulations of the model in this setup are stable in a very large region of the parameter space $g \geq 2$, with in principle no obvious obstacle for simulations at even smaller value of g. The sign problem becomes severe for $g < 5$, which makes measurements unreliable in this region. However, it is very interesting to observe that the sign-reweighting seems *not* to have effect on the measured observables, and it would be important to investigate why this happens further.

Below we investigate two kinds of observables — bosonic and fermionic correlators of the field excitations about the Gubser-Klebanov-Polyakov background [22] — and observe a linear divergence in the measurements of the fermionic masses. This is reminiscent of a typical phenomenon occurring in lattice QCD for quark masses in the case of Wilson fermions, an additive renormalization which manifests itself as a power (linear) divergence in the lattice spacing and it is related to the fact that the lattice action for fermions breaks chiral symmetry (see e.g. [27]). In our case, it is natural to trace back the observed divergence to the fact that our discretization breaks the U(1) part of the original $\mathrm{SO}(6) \times \mathrm{U}(1)$ symmetry of our model. We argue this in details below, using numerics and the relation to the bosonic counterpart of this divergence — the linearly divergent one-point functions of the two AdS excitations transverse to the relevant null cusp classical string solution. The latter are calculated at leading order in lattice perturbation theory in appendix B.

An immediate and crucial outlook of the analysis here presented is the necessity of a redefinition of the continuum limit, which should take into account the infinite mass renormalization observed and therefore a possible tuning of the "bare" mass parameter of the theory (the light-cone momentum P_+, which we redefine as m below). One way to proceed is by studying the violation of the continuum Ward identities on the lattice and explicitly checking that these violations vanish in the continuum limit. It would be also mostly interesting to investigate discretizations of the fermionic action (e.g. inspired to Ginsparg-Wilson fermions) which may preserve a larger symmetry group on the lattice.[3]

This paper proceeds with a presentation of the details on the algebraic manipulation of the Lagrangian and its novel linearization (section 2), an analysis of the spectrum of the fermionic operator (section 3), a study of bosonic and fermionic correlators (section 4) and an analysis of the impact of reweighting procedure on the observables (section 4.2). appendices collect notation and useful details for deriving the fermionic linearization (appendix A) as well as the evaluation at leading order in lattice perturbation theory of the non-trivial one-point function $\langle x \rangle$ (appendix B).

[3]We thank Agostino Patella for discussions on this.

JHEP01(2020)174

2 Linearization and phase-free Pfaffian

The Euclidean superstring action in AdS-lightcone gauge-fixing [20, 21] describing quantum fluctuations around the null-cusp background in $AdS_5 \times S^5$ reads [23]

$$
\begin{aligned}
S_{\text{cusp}} = g \int dtds \, \Bigg\{ & \left| \partial_t x + \frac{1}{2} x \right|^2 + \frac{1}{z^4} \left| \partial_s x - \frac{1}{2} x \right|^2 + \left(\partial_t z^M + \frac{1}{2} z^M + \frac{i}{z^2} z_N \eta_i \left(\rho^{MN}\right)^i{}_j \eta^j \right)^2 \\
& + \frac{1}{z^4} \left(\partial_s z^M - \frac{1}{2} z^M \right)^2 + i \left(\theta^i \partial_t \theta_i + \eta^i \partial_t \eta_i + \theta_i \partial_t \theta^i + \eta_i \partial_t \eta^i \right) - \frac{1}{z^2} \left(\eta^i \eta_i \right)^2 \\
& + 2i \Bigg[\frac{1}{z^3} z^M \eta^i \left(\rho^M\right)_{ij} \left(\partial_s \theta^j - \frac{1}{2} \theta^j - \frac{i}{z} \eta^j \left(\partial_s x - \frac{1}{2} x \right) \right) \\
& + \frac{1}{z^3} z^M \eta_i (\rho^\dagger_M)^{ij} \left(\partial_s \theta_j - \frac{1}{2} \theta_j + \frac{i}{z} \eta_j \left(\partial_s x - \frac{1}{2} x \right)^* \right) \Bigg] \Bigg\}
\end{aligned}
\tag{2.1}
$$

where x, x^* are two bosonic fields transverse to the subspace AdS_3 of the classical solution and z^M $(M = 1, \cdots, 6)$, with $z = \sqrt{z_M z^M}$, are the six cartesian coordinates of the sphere S^5. The Graßmann-odd fields θ_i, η_i, $i = 1, 2, 3, 4$ are complex variables (no Lorentz spinor indices appear) such that $\theta^i = (\theta_i)^\dagger$, $\eta^i = (\eta_i)^\dagger$, transforming in the fundamental representation of the SU(4) R-symmetry group. The matrices ρ^M_{ij} are the off-diagonal blocks of SO(6) Dirac matrices γ^M in chiral representation, and $(\rho^{MN})_i{}^j = (\rho^{[M} \rho^{\dagger N]})_i{}^j$ are the SO(6) generators. Under the U(1) symmetry, the fields z^M are neutral , θ^i and η^i have opposite charges and the charge of η_i (η^i) is half the charge of x (x^*). In the action (2.1) a massive parameter $(\sim P_+)$ is missing, which we restore below in (2.12) defining it as m.

As standard, to take into account the fermionic contribution in the case of higher-order interactions one first linearizes the corresponding Lagrangian, making it quadratic in fermions, and then formally integrates out the Graßmann-odd fields letting their determinant — here, a Pfaffian — to enter the Boltzmann weight of each configuration through re-exponentiation

$$
\int D\Psi \, e^{-\int dtds \, \Psi^T O_F \Psi} = \text{Pf}\, O_F \quad \longrightarrow \quad (\det O_F \, O_F^\dagger)^{\frac{1}{4}} = \int D\xi D\bar{\xi} \, e^{-\int dtds \, \bar{\xi} (O_F O_F^\dagger)^{-\frac{1}{4}} \xi} \,, \tag{2.2}
$$

where the replacement is needed in the case of non-positive-definite Pfaffian.

To linearize, we focus on the part of the Lagrangian in (2.1) which is quartic in fermions

$$
\mathcal{L}_4 = \frac{1}{z^2} \left[-(\eta^2)^2 + \left(i \, \eta_i (\rho^{MN})^i{}_j n^N \eta^j \right)^2 \right] \,, \tag{2.3}
$$

where $n^M = \frac{z^M}{z}$. Notice the plus sign in front of the second term in (2.3), which squares an hermitian bilinear $(i \, \eta_i \rho^{MN\,i}{}_j \eta^j)^\dagger = i \eta_j \, \rho^{MN\,j}{}_i \, \eta^i$ [12]. Then the standard Hubbard-Stratonovich transformation

$$
\begin{aligned}
& \exp \left\{ - g \int dtds \left[- \frac{1}{z^2} \left(\eta^i \eta_i \right)^2 + \left(\frac{i}{z^2} z_N \eta_i \rho^{MN\,i}{}_j \eta^j \right)^2 \right] \right\} \\
& \qquad \sim \int D\phi D\phi^M \, \exp \left\{ - g \int dtds \left[\frac{1}{2} \phi^2 + \frac{\sqrt{2}}{z} \phi \, \eta^2 + \frac{1}{2} (\phi_M)^2 \right. \right. \\
& \qquad\qquad \left. \left. - i \, \frac{\sqrt{2}}{z^2} \phi^M z_N \left(i \, \eta_i \rho^{MN\,i}{}_j \eta^j \right) \right] \right\}
\end{aligned}
\tag{2.4}
$$

JHEP01(2020)174

generates a non-hermitian term, the last one above, resulting in a complex-valued Pfaffian for the fermionic operator. Here we provide a solution to this problem, obtaining a *real-valued* Pfaffian via an alternative procedure, where the first step is rewriting the Lagrangian (2.3) with a procedure inspired by [28]. There, a simpler action with SO(4) four-fermion terms in three dimensions was considered (see also the four-dimensional SU(4) counterpart in [29]). Our Lagrangian (2.3) is invariant under $\mathrm{SU}(4)\times\mathrm{U}(1)$ transformations and this requires a generalization of [28] that preserves this symmetry. Let us start by eliminating the matrices ρ^{MN} from the second term of (2.3) in favour of ρ^{M}, which after some ρ-matrices manipulations leads to

$$\mathcal{L}_4 = \frac{1}{z^2}\left(-4\,(\eta^2)^2 + 2\left|\eta_i(\rho^N)^{ik}n_N\eta_k\right|^2\right) . \tag{2.5}$$

We then define a duality transformation, reminiscent of the standard Hodge duality but adapted to our particular case. Given $\Sigma_i{}^j \equiv \eta_i\eta^j$ the dual matrix $\tilde{\Sigma}_j{}^i$ is defined by

$$\tilde{\Sigma}_j{}^i = n_N n_L(\rho^N)^{ik}(\rho^L)_{jl}\Sigma_k{}^l \ . \tag{2.6}$$

Notice that $\tilde{\tilde{\Sigma}} = \Sigma$ and $\Sigma^i{}_j \equiv (\Sigma_i{}^j)^\dagger = \Sigma_j{}^i$. One can then easily rewrite (2.5) as

$$\mathcal{L}_4 = \frac{2}{z^2}\mathrm{Tr}\left(\Sigma\Sigma + \tilde{\Sigma}\tilde{\Sigma} - \Sigma\tilde{\Sigma}\right) , \tag{2.7}$$

where the trace is over SU(4) fundamental indices. Although we split the first two terms in (2.7) to exhibit the neutrality of the Lagrangian under duality transformation, it is useful to keep in mind that $\mathrm{Tr}\tilde{\Sigma}\tilde{\Sigma} = \mathrm{Tr}\Sigma\Sigma$. Since we want to write down a Lagrangian as the sum of two terms squared, it is natural to introduce the self- and antiself-dual part of Σ

$$\Sigma_\pm = \Sigma \pm \tilde{\Sigma} \tag{2.8}$$

such that $\tilde{\Sigma}_\pm = \pm\Sigma_\pm$. Now the crucial, though elementary fact that $\mathrm{Tr}\Sigma_\pm\Sigma_\pm = 2\mathrm{Tr}\big(\Sigma\Sigma \pm \Sigma\tilde{\Sigma}\big)$ gives us some freedom in the choice of the sign in the Lagrangian,[4] since

$$\mathcal{L}_4 = \frac{1}{z^2}\mathrm{Tr}\left(4\Sigma\Sigma \mp \Sigma_\pm\Sigma_\pm \pm 2\Sigma\Sigma\right) . \tag{2.9}$$

This last equation proves that the complex phase is an artefact of our naive linearization. Indeed, (2.9) provides two equivalent forms of the same action, one which would lead to a phase problem and one which would not. Choosing the latter, i.e. the one involving Σ_+, we obtain for the quartic Lagrangian the expression

$$\mathcal{L}_4 = \frac{1}{z^2}\left(-6\,(\eta^2)^2 - \Sigma_+{}_i^j\Sigma_+{}_j^i\right) . \tag{2.10}$$

[4]It is worth emphasizing that there is neither ambiguity nor arbitrariness in the double sign present in (2.7): writing the Lagrangian in terms of the self-dual part of Σ requires the minus sign, writing it in terms of the antiself-dual part requires the plus sign.

JHEP01(2020)174

In this form the Lagrangian is suitable for the following Hubbard-Stratonovich transformation

$$\begin{aligned}&\exp\left\{-g\int dtds\left[-\frac{1}{z^2}\left(-6\,(\eta^2)^2-\Sigma_{+i}^{\ j}\Sigma_{+j}^{\ i}\right)\right]\right\}\\&\qquad\sim\int D\phi D\phi^M\,\exp\left\{-g\int dtds\left[\frac{12}{z}\eta^2\phi+6\phi^2+\frac{2}{z}\Sigma_{+j}^{\ i}\phi_i^j+\phi_j^i\phi_i^j\right]\right\},\end{aligned}\tag{2.11}$$

where ϕ is real and ϕ_j^i can be thought of as a 4×4 complex hermitian matrix with 16 real degrees of freedom.[5] Therefore the new linearization proposed here introduces a total of 17 auxiliary fields.

The final form of the Lagrangian is then

$$\begin{aligned}\mathcal{L}=&\left|\partial_t x+\frac{m}{2}x\right|^2+\frac{1}{z^4}\left|\partial_s x-\frac{m}{2}x\right|^2+\left(\partial_t z^M+\frac{m}{2}z^M\right)^2\\&+\frac{1}{z^4}\left(\partial_s z^M-\frac{m}{2}z^M\right)^2+6\phi^2+\phi_j^i\phi_i^j+\psi^T O_F\psi\end{aligned}\tag{2.12}$$

with $\psi\equiv\left(\theta^i,\theta_i,\eta^i,\eta_i\right)$ and

$$O_F=\begin{pmatrix}0&\mathrm{i}\partial_t&-\mathrm{i}\rho^M\left(\partial_s+\frac{m}{2}\right)\frac{z^M}{z^3}&0\\ \mathrm{i}\partial_t&0&0&-\mathrm{i}\rho_M^\dagger\left(\partial_s+\frac{m}{2}\right)\frac{z^M}{z^3}\\ \mathrm{i}\frac{z^M}{z^3}\rho^M\left(\partial_s-\frac{m}{2}\right)&0&2\frac{z^M}{z^4}\rho^M\left(\partial_s x-m\frac{x}{2}\right)&\mathrm{i}\partial_t-A^T\\ 0&\mathrm{i}\frac{z^M}{z^3}\rho_M^\dagger\left(\partial_s-\frac{m}{2}\right)&\mathrm{i}\partial_t+A&-2\frac{z^M}{z^4}\rho_M^\dagger\left(\partial_s x^*-m\frac{x}{2}{}^*\right)\end{pmatrix},\tag{2.13}$$

where

$$A=-\frac{6}{z}\phi+\frac{1}{z}\tilde{\phi}+\frac{1}{z^3}\rho_N^*\tilde{\phi}^T\rho^L z^N z^L+\mathrm{i}\frac{z^N}{z^2}\rho^{MN}\partial_t z^M,\qquad\tilde{\phi}\equiv\left(\tilde{\phi}_{ij}\right)\equiv\left(\phi_j^i\right).\tag{2.14}$$

The discretization that we will adopt here was presented in [12]. There, it was observed that it is a priori not possible to remove fermion doublers while maintaining all the symmetries of the model and preventing complex phases to appear in the determinant. A "minimal-breaking" solution preserves the SU(4) global symmetry of the Lagrangian and *breaks* the U(1),[6] and it consists in adding a Wilson-like term in the main diagonal of the fermionic operator. In lattice perturbation theory, this discretization reproduces in the continuum limit $a\to0$ the large g, one-loop value of the cusp anomalous dimension [12]. As the new linearization affects off-diagonal terms (A-terms), we can simply proceed with the proposal in [12] for the discretized fermionic operator

$$\hat{O}_F=\begin{pmatrix}W_+&-\mathring{p}_0\mathbb{1}&(\mathring{p}_1-i\frac{m}{2})\rho^M\frac{z^M}{z^3}&0\\ -\mathring{p}_0\mathbb{1}&-W_+^\dagger&0&\rho_M^\dagger(\mathring{p}_1-i\frac{m}{2})\frac{z^M}{z^3}\\ -(\mathring{p}_1+i\frac{m}{2})\rho^M\frac{z^M}{z^3}&0&2\frac{z^M}{z^4}\rho^M\left(\partial_s x-m\frac{x}{2}\right)+W_-&-\mathring{p}_0\mathbb{1}-A^T\\ 0&-\rho_M^\dagger(\mathring{p}_1+i\,\frac{m}{2})\frac{z^M}{z^3}&-\mathring{p}_0\mathbb{1}+A&-2\frac{z^M}{z^4}\rho_M^\dagger\left(\partial_s x^*-m\frac{x}{2}{}^*\right)-W_-^\dagger\end{pmatrix}\tag{2.15}$$

[5] The proof of (2.11) is based on these properties, the split of $\Sigma_{+i}^{\ j}$ and ϕ_j^i with $i\neq j$ into real and imaginary parts and the Gaussian integration formula over real variables.

[6] Another possible discretization, also used in [12], breaks both SO(6) and U(1) symmetries.

JHEP01(2020)174

with [27]

$$\mathring{p}_\mu = \frac{1}{a}\sin(p_\mu a)\,, \qquad\qquad \hat{p}_\mu \equiv \frac{2}{a}\sin\frac{p_\mu a}{2}\,, \tag{2.16}$$

A is in our case defined in (2.14), and ($|r| = 1$)

$$W_\pm = \frac{r}{2\,z^2}\left(\hat{p}_0^2 \pm i\,\hat{p}_1^2\right)\rho^M z_M\,. \tag{2.17}$$

We recall that the U(1) symmetry forbids in the original action the presence of bilinears made up of fermions with identical U(1) charge (upper diagonal block entries in (2.13)), and only allows them if some compensating, oppositely charged, field multiplies them (lower diagonal block entries in (2.13)). The Wilson term $W_\pm$ in (2.17) is U(1)-neutral, and the breaking of the U(1) symmetry is due to its presence in the diagonal of (2.15).

The values of the discretised (scalar) fields are assigned to each lattice site, with periodic boundary conditions for all the fields except for antiperiodic temporal boundary conditions in the case of fermions.

3 Spectrum of the fermionic operator

In simpler cases of models with four-fermion interactions [28, 29] a choice of Yukawa terms similar in spirit to the one described in the previous section turns out to ensure a positive-definite Pfaffian. There the relevant operator is real and antisymmetric — so that its purely imaginary eigenvalues come in pairs $(i\,a, -ia)$ — *and* the symmetries of the model ensure that all eigenvalues are also doubly degenerate. One may then define the Pfaffian as the product of eigenvalues with positive imaginary part on the initial configuration. As the simulation progresses, sign flips in the Pfaffian correspond to an odd number of eigenvalues crossing through the origin, but as all eigenvalues are doubly degenerate such sign changes cannot occur. For a system with a positive-definite Pfaffian the arrow in (2.2) is an equivalence, and no sign problem appears.

In our case, the fermionic operator $\hat{O}_F$ is antisymmetric, and satisfies the constraint (reminiscent of the γ_5-hermiticity in lattice QCD) [11, 12]

$$\hat{O}_F^\dagger = \Gamma_5\,\hat{O}_F\,\Gamma_5\,, \tag{3.1}$$

where Γ_5 is the following unitary, antihermitian matrix

$$\Gamma_5 = \begin{pmatrix} 0 & \mathbb{1} & 0 & 0 \\ -\mathbb{1} & 0 & 0 & 0 \\ 0 & 0 & 0 & \mathbb{1} \\ 0 & 0 & -\mathbb{1} & 0 \end{pmatrix}\,, \qquad \Gamma_5^\dagger\Gamma_5 = \mathbb{1} \qquad \Gamma_5^\dagger = -\Gamma_5\,. \tag{3.2}$$

The antisymmetry and the property (3.1) ensure $\det\hat{O}_F$ to be *real* and *non-negative*. While the absence of a complex phase allows us to eliminate a systematic error of our previous analysis, it is not enough to make the Pfaffian positive-definite, implying that the model may still suffer a sign problem. One can check that — in the case of generally complex eigenvalues λ — the antisymmetry and the Γ_5-hermiticity (3.1) ensure a spectrum

JHEP01(2020)174

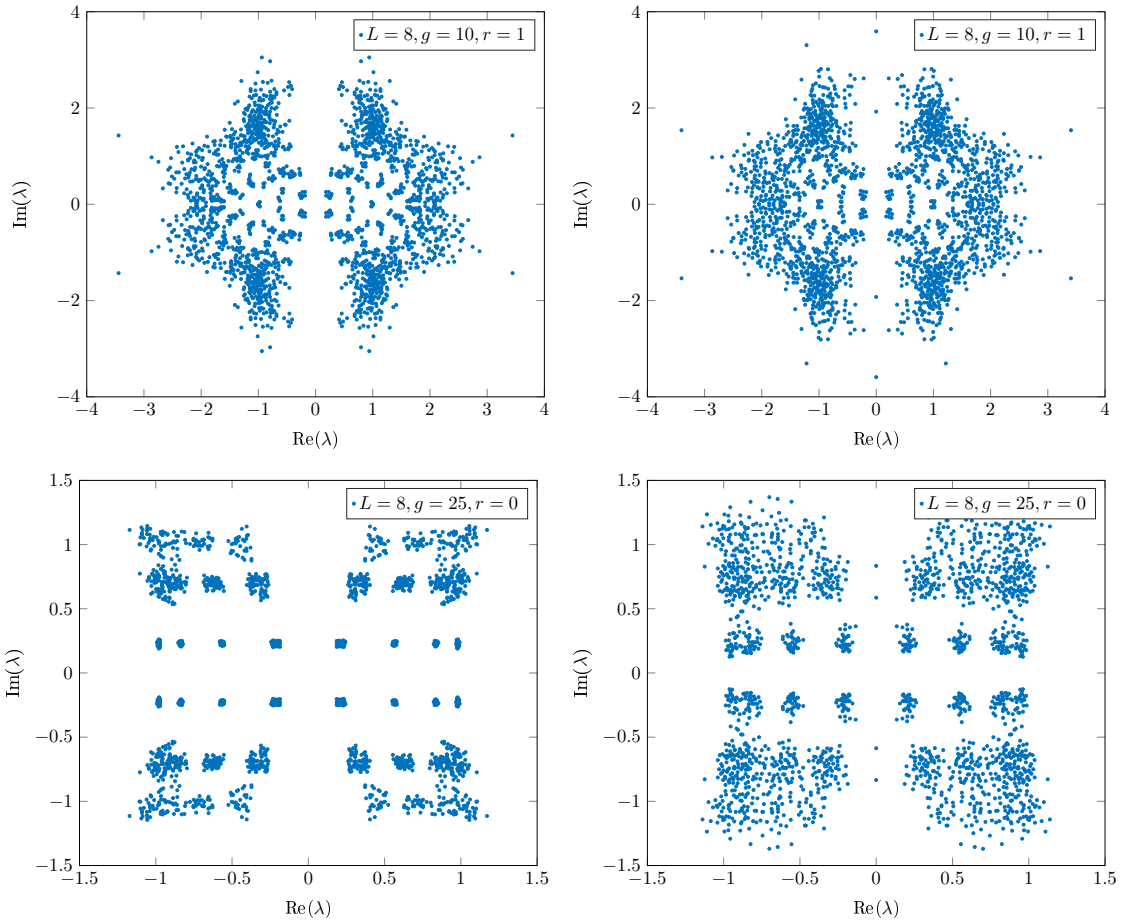

Figure 1. Spectrum of $\hat{O}_F$, in absence (left diagrams) and presence (right diagrams) of A (Yukawa-like) terms.

characterized by *quartets* $(\lambda, -\lambda^*, -\lambda, \lambda^*)$. One can then define the Pfaffian on the starting configuration as the product $(\lambda\,\lambda^*)$ for each quartet, which would provide sign flips in $\mathrm{Pf}\hat{O}_F$. However, for purely imaginary or purely real eigenvalues, the disposition in quartets is no longer enforced by (3.1) and indeed may not happen, leaving a spectrum of pairs $(\lambda, -\lambda)$ with no degeneracy. A numerical study of the spectrum of $\hat{O}_F$ appears to indicate that the disposition in quartets would occur if the A-terms in (2.13) — defining Yukawa-like terms — were vanishing, see figure 1 left, while for $A \neq 0$ (on the right) purely imaginary eigenvalues may appear, with no degeneracy. One should notice that such purely imaginary eigenvalues appear also when auxiliary fields are set to zero — and thus the only non-vanishing A-term is the one present in the original Lagrangian, before linearization — suggesting that the sign ambiguity cannot be tamed by a suitably-enough choice of auxiliary fields.

A sign problem appears already at $g = 5$ [12], and figure 2 (left panel) shows that the problem becomes severe for values of the coupling $g \sim 2$. It is interesting to look at the lowest eigenvalue for the squared fermionic operator $\hat{O}_F^\dagger \hat{O}_F$ in a large region of the parameter space. If zero eigenvalues of $\hat{O}_F^\dagger \hat{O}_F$ do not occur for certain values of the parameters, no zero eigenvalues will occur for $\hat{O}_F$ as well, and thus no sign flips for its Pfaffian. The

JHEP01(2020)174

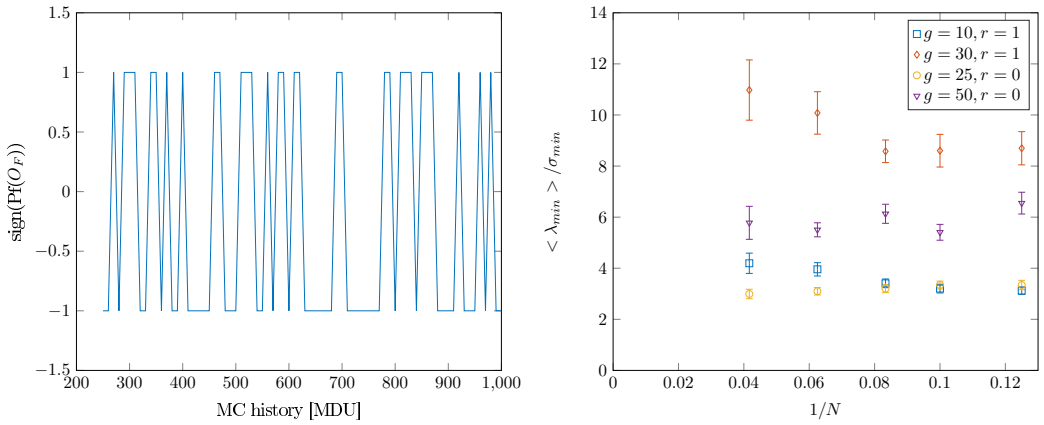

Figure 2. *Left panel:* Monte Carlo history for the sign of the Pfaffian of O_F in (2.13) at a value $g = 2$ of the coupling. The strong oscillatory behavior indicates a severe sign problem. *Right panel:* the lowest eigenvalue $\lambda_{\min}$ for the squared fermionic operator $O_F^\dagger O_F$ appears to be well separated from zero, a statement which then also holds for O_F. The variance is defined by $\sigma^2_{\min} = \langle \lambda^2_{\min} \rangle - \langle \lambda_{\min} \rangle^2$. In the region of parameters explored, no zero eigenvalues for $\det O_F$ appear, indicating that for the *real* Pfaffian $\mathrm{Pf} O_F$ no sign flips should occur.

right panel of figure 2 shows that the smallest eigenvalues of $\hat{O}_F^\dagger \hat{O}_F$ are clearly separated from zero for values of $g \gtrsim 10$. Although not a proof of their absence, this "gap" suggest that sign flips are extremely unlikely. It would be interesting to understand the reason for this "gap". It is also interesting to notice that this region of the parameter space safely includes $g = 10$, at which simulations [12] appear to detect a non-perturbative behavior.[7]

4 Simulations at finite coupling

We will now explore the region of the coupling $g < 10$, where a sign problem appears. In addition to the latter, simulations at $g \lesssim 5$ run into numerical instabilities due to the non-convergence of the inverter for the fermionic matrix. These instabilities can be traced back to the presence of zero eigenvalues of the fermionic operator, and may be cured by regularizing the fermionic Pfaffian in a way reminiscent of the twisted-mass reweighting procedure of [26] (see also [30]). Namely, a massive term is added to the fermionic matrix to obtain

$$\tilde{O}_F = \hat{O}_F + i\,\mu\,\Gamma_5\,, \qquad \tilde{O}_F \tilde{O}_F^\dagger = \hat{O}_F \hat{O}_F^\dagger + \mu^2\,\mathbb{1}\,, \tag{4.1}$$

so that $\mu^2\,\mathbb{1}$ shifts the eigenvalues of $\hat{O}_F \hat{O}_F^\dagger$ apart from zero. To compensate for this, one uses reweighting (see below) and refers to μ as the reweighting mass parameter.

Therefore, in this region of the parameter space simulations are not done with the exact string worldsheet action as given by the discretized version of (2.12) and (2.13) (in configuration space), but differ due to both the replacement (2.2) of the Pfaffian by its absolute value *and* the addition of the "twisted mass" in (4.1). The expectation values

[7] We refer here to the measurement of the derivative of the cusp anomaly studied in [12], which show a clear downward behavior — non-perturbative — for $g = 10$ and beyond.

JHEP01(2020)174

$\langle\mathcal{O}\rangle$ of observables in the underlying, target theory are then obtained from the expectation values $\langle O\rangle_{\rm m}$ in the theory with the modified, positive-definite fermionic determinant $(\det\left(\tilde{O}_F\tilde{O}_F^\dagger\right)+\mu^2)^{\frac{1}{4}}$ as follows

$$\langle\mathcal{O}\rangle = \frac{\langle\mathcal{O}\,W\rangle_{\rm m}}{\langle W\rangle_{\rm m}}\,, \tag{4.2}$$

where the total reweighting factor W reads in our case[8]

$$W = W_{\rm s}\,W_\mu\,, \qquad W_s = \text{sign}\,\text{Pf}\,\hat{O}_F \qquad W_\mu = \frac{(\det\hat{O}_F^\dagger\,\hat{O}_F)^{\frac{1}{4}}}{\left(\det(\hat{O}_F^\dagger\,\hat{O}_F+\mu^2)\right)^{\frac{1}{4}}}\,. \tag{4.3}$$

Below we will investigate two kinds of observables (bosonic and fermionic correlators) and evaluate the reweighting factors exactly, which is feasible in the case of small lattices. We will choose for μ two different values, and comment on the impact of reweighting on the observables.

For a part of this paper (see section 3 and section 4.2) we work at finite, relatively small values of N, which allows to use exact algorithms for evaluating with reasonable effort fermion determinants or Pfaffians. In particular, we employ the algorithm in [31] to evaluate the Pfaffian of a matrix without reference to its determinant. All the analysis in section 4.1 the Pfaffian is evaluated stochastically within a rational hybrid Monte Carlo algorithm. In order to simulate at a point where finite volume effects are small we fix parameters and thus the line of constant physics in the bare parameter space as in [12]. Namely, in the space of parameters (g, N, M) — the dimensionless coupling $g = \frac{\sqrt{\lambda}}{4\pi}$, the number of lattice points N and the dimensionless "mass" parameter $M = m\,a$ — we keep $L\,m \equiv NM = \text{const} \equiv 4$. The continuum limit is then taken in this paper via a simple extrapolation to $N \to \infty$. One of the main conclusions of this paper is that this line of constant physics needs to be modified, in view of an infinite renormalization occurring for the fermionic masses. Error bars in the plots below represent statistical errors and include effects of auto-correlation in the Monte Carlo data [32].

Table 1 collects the parameters of the simulations here presented. Configurations are generated by the standard Rational Hybrid Monte Carlo (RHMC) algorithm [33, 34], with a rational approximation of degree 15 for the inverse fractional power in (2.2).

4.1 Observables

4.1.1 The $\langle xx^*\rangle$ correlator

We use the new linearization of the (discretized) Lagrangian (2.12) with (2.14)–(2.17) to repeat the analysis for the mass of the bosonic field x in section 4.1 of [12]. Here, we defined the timeslice correlation function on the lattice at given time interval t

$$C_x(t;k) \equiv \sum_{s,s'} e^{-ik(s_1-s_2)} G_x(t,s,0,s') \tag{4.4}$$

[8] Given the exploratory nature of our study, we do not address here a further (so-called RHMC) reweighting factor accounting for the accuracy of the rational approximation for the inversion $(\hat{O}_F\hat{O}_F^\dagger)^{-\frac{1}{4}}$ in (2.2).

JHEP01(2020)174

g	$T/a \times L/a$	Lm	am	μ
2	16×8	4	0.50000	0.01
5	16×8	4	0.50000	0.01
5	16×8	4	0.50000	0.02
10,20,25,30,50,100	16×8	4	0.50000	0.0
	20×10	4	0.40000	0.0
	24×12	4	0.33333	0.0
	32×16	4	0.25000	0.0
	48×24	4	0.16667	0.0
	64×32	4	0.12500	0.0

Table 1. The parameters of our simulations are the coupling g, the temporal (T) and spatial (L) extent of the lattice in units of the lattice spacing a. The mass parameter am is given by the fixing the combination $Lm = 4$. The reweighting parameter μ is non-zero only for $g < 10$.

from the *connected* two-point function

$$G_x(t, s, t', s') \equiv \langle x(t, s) x^*(t', s') \rangle_{\rm c} = \langle x(t, s) x^*(t', s') \rangle - \langle x(t, s) \rangle \langle x^*(t', s') \rangle \ . \tag{4.5}$$

The subtraction of the one-point functions is irrelevant in the continuum, where the U(1) invariance implies $\langle x \rangle = \langle x^* \rangle = 0$, but is crucial on the lattice, where the Wilson term breaks this symmetry. The non-trivial, and linearly divergent, one-point functions of $\tilde{x}$, $\tilde{x}^*$ are calculated at leading order in lattice perturbation theory in appendix B. In figure 3 we show the plot of $\langle x \rangle$ for several values of g and N.

The exponential fall-off of the timeslice correlator for large interval t and zero momentum defines the physical mass of the fluctuation x

$$C_x(t;\, 0) \ \overset{t \gg 1}{\sim} \ e^{-t\, m_{x\rm LAT}} \ . \tag{4.6}$$

On the lattice the periodic boundary condition on the field x in the time direction imposes the relation $C_x(t) = C_x(T - t)$, which means that (4.6) is rather

$$C_x(t;\, 0) \ \overset{t \gg 1}{\sim} \ e^{-t m_{x\rm LAT}} + e^{-(T-t) m_{x\rm LAT}} \ . \tag{4.7}$$

The value of the physical mass is measured, on the lattice, from the limit of an effective mass $m_x^{\rm eff}$ for fixed lattice time extension T

$$m_{x\rm LAT} = \lim_{T,\, t \to \infty} m_x^{\rm eff} \ . \tag{4.8}$$

We estimate the latter by fitting the timeslice correlator $C_x(t; 0)$ with a double exponential

$$A \Big[e^{-t m_x^{\rm eff}} + e^{-(T-t) m_x^{\rm eff}} \Big] \tag{4.9}$$

on the interval $1 \ll t \ll T$. The overall factor A is irrelevant; measurements of $m_x^{\rm eff}$ improve when $T = 2L$ and data points at $t \sim T/2$, which are affected by the largest relative errors,

JHEP01(2020)174

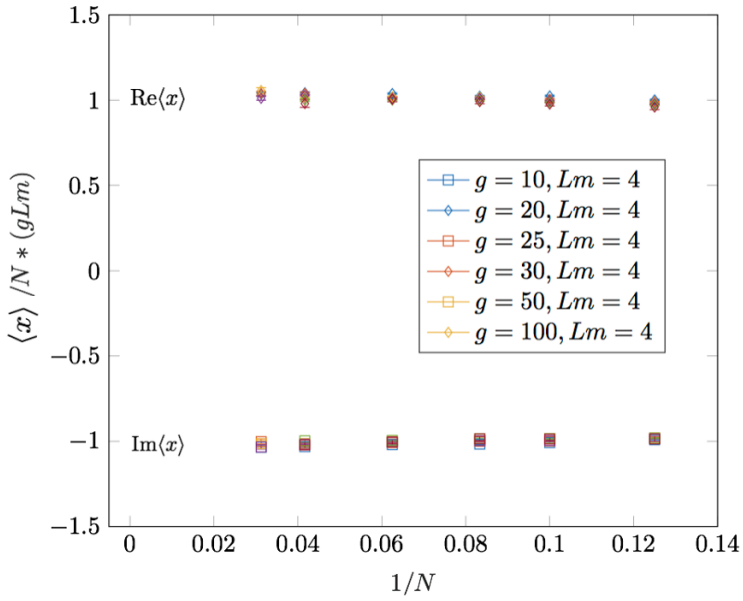

Figure 3. Plot of the real and imaginary part of $\langle x \rangle$ for several values of g and N. The vacuum expectation value is normalized by $N/(gLm)$, namely the perturbation theory result (B.10) at $\mathcal{O}(1/g)$, and therefore the constant behavior visible in the flatness shows for $\langle x \rangle$ a divergence which is *linear* in N.

are discarded. A major source of uncertainty comes from the estimate of the one-point functions in (4.5), which is reduced as follows. Denoting the Fourier component of x at zero spatial momentum by

$$\tilde{x}(t) \equiv \sum_s x(t,s) \tag{4.10}$$

and splitting the field x into real $x_{\rm R}$ and imaginary part $x_{\rm I}$, the connected timeslice correlator (4.4) takes the form

$$\begin{aligned}\langle \tilde{x}(t)\tilde{x}^*(0)\rangle_{\rm c} = {} & \langle \tilde{x}_{\rm R}(t)\tilde{x}_{\rm R}(0)\rangle + \langle \tilde{x}_{\rm I}(t)\tilde{x}_{\rm I}(0)\rangle - \langle \tilde{x}_{\rm R}(t)\rangle\langle \tilde{x}_{\rm R}(0)\rangle - \langle \tilde{x}_{\rm I}(t)\rangle\langle \tilde{x}_{\rm I}(0)\rangle \\ & + i\left(\langle \tilde{x}_{\rm I}(t)\tilde{x}_{\rm R}(0)\rangle - \langle \tilde{x}_{\rm R}(t)\tilde{x}_{\rm I}(0)\rangle\right) .\end{aligned} \tag{4.11}$$

The second line vanishes due to translational and time-reversal invariance. In appendix B we show that it holds

$$\langle \tilde{x}_{\rm R}\rangle = -\langle \tilde{x}_{\rm I}\rangle , \tag{4.12}$$

while the relations[9]

$$\langle \tilde{x}_{\rm R}(t)\,\tilde{x}_{\rm I}(0)\rangle = \langle \tilde{x}_{\rm R}(t)\rangle\langle \tilde{x}_{\rm I}(0)\rangle , \qquad \langle \tilde{x}_{\rm I}(t)\,\tilde{x}_{\rm R}(0)\rangle = \langle \tilde{x}_{\rm I}(t)\rangle\langle \tilde{x}_{\rm R}(0)\rangle \tag{4.13}$$

are observed to hold within numerical precision. These last two equations allow us to trade the disconnected pieces in (4.11) with connected ones, e.g. $\langle \tilde{x}_{\rm R}(t)\rangle\langle \tilde{x}_{\rm R}(0)\rangle = -\langle \tilde{x}_{\rm R}(t)\tilde{x}_{\rm I}(0)\rangle$, which brings (4.11) into the form

$$C_x(t;\,0) = \langle \tilde{x}_{\rm R}(t)\tilde{x}_{\rm R}(0) + \tilde{x}_{\rm I}(t)\tilde{x}_{\rm I}(0) + \tilde{x}_{\rm R}(t)\tilde{x}_{\rm I}(0) + \tilde{x}_{\rm I}(t)\tilde{x}_{\rm R}(0)\rangle \tag{4.14}$$

[9]The second equation follows from the first for translational invariance.

JHEP01(2020)174

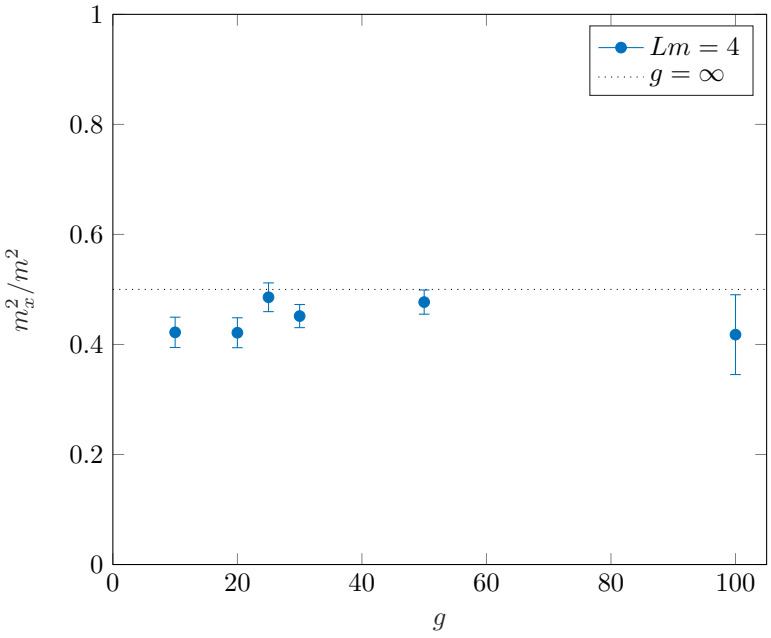

Figure 4. Continuum values for the measured x mass versus g (blue dots). The extrapolation of the values at finite lattice spacing to the continuum limit is performed as in [12]. The dotted line is the $g \to \infty$ limit of the continuum prediction.

and substantially reduces the statistical error. Figure (4) shows the measured x mass, as extrapolated in the continuum from (4.8). The estimate is consistent with the large g, continuum prediction $m_x^2(g) = \frac{m^2}{2}\left(1 - \frac{1}{8\,g} + \mathcal{O}(g^{-2})\right)$ (see discussion in [12]). As already noticed in [12], there appears to be no infinite renormalization occurring for m_x^2. As we will see below in section (4.1.2), however, this is not the case for the fermionic masses, implying that eventually the bare parameter m will have to be tuned to adjust for it and the continuum limit will have to be reformulated.

4.1.2 The fermionic correlators

The fermionic generating functional on the lattice is defined by

$$\begin{aligned} Z_F^{\rm LAT}[J] &\equiv \int [D\psi]\, e^{\frac{1}{2}\sum_{t,s,t',s'} \psi^T(t,s)\, O_F(t,s,t',s')\, \psi(t',s') + \sum_{t,s} \psi^T(t,s)\, J(t,s)} \\ &= {\rm Pf}(O_F)\, e^{\frac{1}{2}\sum_{t,s,t',s'} J^T(t,s)\, O_F^{-1}(t,s,t',s')\, J(t',s')} \end{aligned} \tag{4.15}$$

and evaluated for a given configuration of the bosonic fields. J is a 16-component vector of Grassmann-valued source fields conjugated to the fermionic field $\psi = (\theta^i, \theta_i, \eta^i, \eta_i)$ with $i, j = 1, \ldots 4$, and sums run over the lattice sites indexed by $t = 1, \ldots 2N$ and $s = 1, \ldots N$. Fermionic two-point functions are obtained differentiating (4.15) with respect to $J^{\hat{i}}$ with $\hat{i}, \hat{j} = 1, \ldots 16$

$$\frac{\partial}{\partial J^{\hat{i}}(t,s)} \frac{\partial}{\partial J^{\hat{j}}(t',s')} Z_F^{\rm LAT}[J]\Big|_{J=0} = {\rm Pf}(O_F)\, [O_F^{-1}(t,s,t',s')]_{\hat{i}\hat{j}} \tag{4.16}$$

JHEP01(2020)174

and integrated over the bosonic fields to obtain the relation

$$G_{\psi_{\hat{i}}\psi_{\hat{j}}}(t,s,t',s') \equiv \langle \psi_{\hat{i}}(t,s)\psi_{\hat{j}}(t',s')\rangle = \langle [O_F^{-1}(t,s,t',s')]_{\hat{i}\hat{j}}\rangle \ . \tag{4.17}$$

For the various components we extract the following two-point functions

$$\begin{aligned}
&G_{\theta^i\theta^j}(t,s,t',s') = \langle [O_F^{-1}(t,s,t',s')]_{i,j}\rangle \ , && G_{\theta^i\theta_j}(t,s,t',s') = \langle [O_F^{-1}(t,s,t',s')]_{i,j+4}\rangle \ , \\
&G_{\eta^i\eta^j}(t,s,t',s') = \langle [O_F^{-1}(t,s,t',s')]_{i+8,j+8}\rangle \ , && G_{\eta^i\eta_j}(t,s,t',s') = \langle [O_F^{-1}(t,s,t',s')]_{i+8,j+12}\rangle \ , \\
&G_{\theta^i\eta^j}(t,s,t',s') = \langle [O_F^{-1}(t,s,t',s')]_{i,j+8}\rangle \ , && G_{\theta^i\eta_j}(t,s,t',s') = \langle [O_F^{-1}(t,s,t',s')]_{i,j+12}\rangle \ .
\end{aligned} \tag{4.18}$$

In analogy with (4.5), to evaluate the mass we define timeslice correlators of fermionic fields on the lattice as

$$C^{\rm LAT}_{\psi^{\hat{i}}\psi^{\hat{j}}}(t;k) = \sum_{s_1,s_2} e^{-ik(s_1-s_2)} G_{\psi^{\hat{i}}\psi^{\hat{j}}}(t,s_1,0,s_2) \tag{4.19}$$

and project on the zero spacial momentum $k=0$.

As usual, it is instructive to start considering the perturbative region. At large g, the inverse of the fermionic operator (2.13) in momentum-space representation reads

$$K_F^{-1}(p_0,p_1) = [{\rm det}K_F(p_0,p_1)]^{-1/8}\, \hat{K}_F^{\dagger}(p_0,p_1) \tag{4.20}$$

where

$$[{\rm det}K_F(p_0,p_1)]^{1/8} = \mathring{p}_0{}^2 + \mathring{p}_1{}^2 + \frac{m^2}{4} + \frac{a^2\, r^2}{4}\left(\hat{p}_0^4 + \hat{p}_1^4\right) \tag{4.21}$$

and

$$\hat{K}_F^{\dagger}(p_0,p_1) = \begin{pmatrix}
\frac{r}{2}\left(\hat{p}_0^2 - i\hat{p}_1^2\right)\rho_M^{\dagger}u^M & -\mathring{p}_0\mathbb{1} & -\left(\mathring{p}_1 - i\frac{ma}{2}\right)\rho_M^{\dagger}u^M & 0 \\
-\mathring{p}_0\mathbb{1} & -\frac{r}{2}\left(\hat{p}_0^2 + i\hat{p}_1^2\right)\rho_M u^M & 0 & -\left(\mathring{p}_1 - i\frac{ma}{2}\right)\rho_M u^M \\
\left(\mathring{p}_1 + i\frac{ma}{2}\right)\rho_M^{\dagger}u^M & 0 & \frac{r}{2}\left(\hat{p}_0^2 + i\hat{p}_1^2\right)\rho_M^{\dagger}u^M & -\mathring{p}_0\mathbb{1} \\
0 & \left(\mathring{p}_1 + i\frac{ma}{2}\right)\rho_M u^M & -\mathring{p}_0\mathbb{1} & -\frac{r}{2}\left(\hat{p}_0^2 - i\hat{p}_1^2\right)\rho_M u^M
\end{pmatrix} \tag{4.22}$$

and we temporarily reinstated the lattice spacing a. The inverse Fourier transform of the matrix entries of (4.20) over the time-like momentum component

$$C_{\psi_{\hat{i}}\psi_{\hat{j}}}(t,p_1) = \frac{a}{g}\int_{-\infty}^{\infty} dp_0\, e^{ip_0 t}[K_F^{-1}(p_0,p_1)]_{\hat{i}\hat{j}} \tag{4.23}$$

yields the following analytic predictions for the timeslice correlators (4.19) at $g \gg 1$

$$C_{\theta^i\theta^j}(t;0) = C_{\eta^i\eta^j}(t;0) = \frac{-\pi\, u^M \left(\rho_M^{\dagger}\right)^{ij}}{g\sqrt{4-m^2a^2r^2}}\left[\bar{V}_- \exp\left(-\frac{t}{ar}\bar{V}_-\right) - \bar{V}_+ \exp\left(-\frac{t}{ar}\bar{V}_+\right)\right] \tag{4.24}$$

JHEP01(2020)174

$$C_{\theta_i\theta_j}(t;0) = C_{\eta_i\eta_j}(t;0) = \frac{\pi\, u^M\,(\rho_M)_{ij}}{g\,\sqrt{4-m^2a^2r^2}}\left[\bar{V}_-\exp\left(-\frac{t}{ar}\bar{V}_-\right) - \bar{V}_+\exp\left(-\frac{t}{ar}\bar{V}_+\right)\right] \tag{4.25}$$

$$\begin{aligned} C_{\theta^i\theta_j}(t;0) &= C_{\theta_i\theta^j}(t;0) = C_{\eta^i\eta_j}(t;0) \\ &= C_{\eta_i\eta^j}(t;0) = \frac{-2\pi i\delta_{ij}}{g\,\sqrt{4-m^2a^2r^2}}\left[\exp\left(-\frac{t}{ar}\bar{V}_-\right) - \exp\left(-\frac{t}{ar}\bar{V}_+\right)\right] \end{aligned} \tag{4.26}$$

$$C_{\theta^i\eta^j}(t;0) = C_{\eta^i\theta^j}(t;0) = \frac{ima\pi r\, u^M\left(\rho_M^\dagger\right)^{ij}}{g\,\sqrt{4-m^2a^2r^2}}\left[\frac{\exp\left(-\frac{t}{ar}\bar{V}_-\right)}{\bar{V}_-} - \frac{\exp\left(-\frac{t}{ar}\bar{V}_+\right)}{\bar{V}_+}\right] \tag{4.27}$$

$$C_{\theta_i\eta_j}(t;0) = C_{\eta_i\theta_j}(t;0) = \frac{ima\pi r\, u^M\,(\rho_M)_{ij}}{g\,\sqrt{4-m^2a^2r^2}}\left[\frac{\exp\left(-\frac{t}{ar}\bar{V}_-\right)}{\bar{V}_-} - \frac{\exp\left(-\frac{t}{ar}\bar{V}_+\right)}{\bar{V}_+}\right] \tag{4.28}$$

$$C_{\theta^i\eta_j}(t;0) = C_{\theta_i\eta^j}(t;0) = C_{\eta^i\theta_j}(t;0) = C_{\eta_i\theta^j}(t;0) = 0 \tag{4.29}$$

with

$$\bar{V}_\pm = \sqrt{2\pm\sqrt{4-m^2a^2r^2}}\,. \tag{4.30}$$

In the continuum limit ($a\to 0$) $\bar{V}_+ = 2+\mathcal{O}(a^2)$ and $\bar{V}_- \sim \frac{a\,m\,r}{2}$. Therefore, of the exponentials $\exp\left(-\frac{t}{ar}\bar{V}_\pm\right)$, only the ones with $\bar{V}_-$ survive. The propagators in the first two lines above vanish in the limit, while the remaining (non-vanishing) correlators reduce to a single exponential

$$C_{\theta^i\theta_j}(t;0) = C_{\theta_i\theta^j}(t;0) = C_{\eta^i\eta_j}(t;0) = C_{\eta_i\eta^j}(t;0) = -\frac{\pi i}{g}\,\delta^i_j\exp\left(-\frac{tm}{2}\right) \tag{4.31}$$

$$C_{\theta^i\eta^j}(t;0) = C_{\eta^i\theta^j}(t;0) = \frac{i\pi}{g}\,u^M\left(\rho_M^\dagger\right)^{ij}\exp\left(-\frac{tm}{2}\right) \tag{4.32}$$

$$C_{\theta_i\eta_j}(t;0) = C_{\eta_i\theta_j}(t;0) = \frac{i\pi}{g}\,u^M\,(\rho_M)_{ij}\exp\left(-\frac{tm}{2}\right), \tag{4.33}$$

in agreement with the continuum results [23]. Notice that the prediction based on the integrability of the model (namely, the study of the dispersion relations for these modes [35] via the asymptotic Bethe Ansatz) is that that the masses of the fermionic fields should not get renormalized, holding their value $m/2$ for all values of the coupling.

For our measurements we consider the diagonal correlators (4.31). In fact, to reduce the variance we use the SU(4) $\sim$ SO(6) symmetry and look at their averaged values

$$C_{\theta\theta}(t) = \frac{1}{8}\sum_{i,j}\left[\,C_{\theta^i\theta_i}(t) + C_{\theta_i\theta^i}(t)\,\right], \tag{4.34}$$

$$C_{\eta\eta}(t) = \frac{1}{8}\sum_{i,j}\left[\,C_{\eta^i\eta_i}(t) + C_{\eta_i\eta^i}(t)\,\right]. \tag{4.35}$$

and at the sum $C_{\rm sum} = (C_{\theta\theta} + C_{\eta\eta})/2$. The discussion above suggests to fit the Monte Carlo data to a single exponential decay, similar to (4.9). Such fits were tried but rejected

JHEP01(2020)174

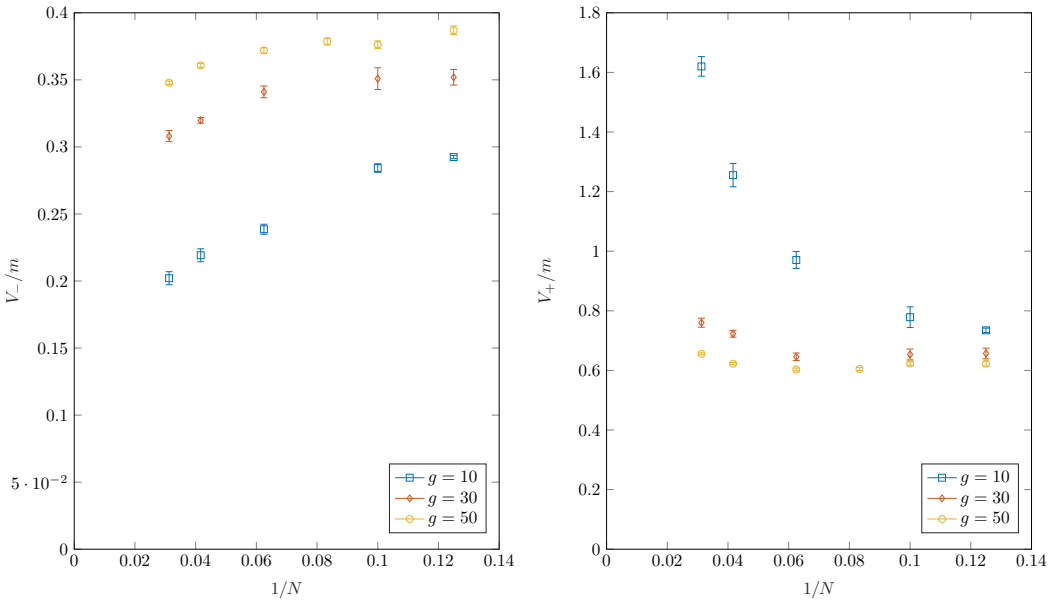

Figure 5. The exponential decays resulting from the fit of the Monte Carlo data for the fermionic correlators C_{sum} to (4.36) for $g = 10, 30, 50$ and various values of N.

because of their large χ^2 values of the chi-squared test. However, as will become clear below, the data from finite lattices with temporal extent T and anti-periodic boundary conditions can be fitted to the function

$$C_{\text{sum}}(t) \sim \; e^{-t\,V_-} + e^{-t\,V_+} + (t \to T - t)\,. \tag{4.36}$$

As shown in figure 5, a linear ($\sim N$) divergence and a strong dependence on the coupling g appears in the measured "masses" V_+ and V_- above. A natural guess is to relate this divergence to the U(1) symmetry-breaking of our discretization, considering this as the fermionic counterpart of the bosonic effect $\langle x \rangle \neq 0$ which is also linearly divergent — see section 4.1.1 and discussion below (4.5). In fact, we may perform even in the continuum the simple exercise of evaluating these correlators on a vacuum with $\langle x \rangle \neq 0$. Then at tree level the diagonal fermionic correlators read

$$\begin{aligned} C_{\theta\theta}(t)_{\langle x\rangle\neq 0} \sim \frac{1}{2}\left(1 + \frac{2\left|\partial_s\langle x\rangle - m\frac{\langle x\rangle}{2}\right|}{\sqrt{4\left|\partial_s\langle x\rangle - m\frac{\langle x\rangle}{2}\right|^2 + m^2}}\right) e^{-t\,\widetilde{V_-}} \\ + \frac{1}{2}\left(1 - \frac{2\left|\partial_s\langle x\rangle - m\frac{\langle x\rangle}{2}\right|}{\sqrt{4\left|\partial_s\langle x\rangle - m\frac{\langle x\rangle}{2}\right|^2 + m^2}}\right) e^{-t\,\widetilde{V_+}} \end{aligned} \tag{4.37}$$

$$\begin{aligned} C_{\eta\eta}(t)_{\langle x\rangle\neq 0} \sim \frac{1}{2}\left(1 - \frac{2\left|\partial_s\langle x\rangle - m\frac{\langle x\rangle}{2}\right|}{\sqrt{4\left|\partial_s\langle x\rangle - m\frac{\langle x\rangle}{2}\right|^2 + m^2}}\right) e^{-t\,\widetilde{V_-}} \\ + \frac{1}{2}\left(1 + \frac{2\left|\partial_s\langle x\rangle - m\frac{\langle x\rangle}{2}\right|}{\sqrt{4\left|\partial_s\langle x\rangle - m\frac{\langle x\rangle}{2}\right|^2 + m^2}}\right) e^{-t\,\widetilde{V_+}} \end{aligned} \tag{4.38}$$

JHEP01(2020)174

with

$$\widetilde{V}_{\pm} = \sqrt{\frac{m^2}{4} + 2\left|\partial_s\langle x\rangle - m\frac{\langle x\rangle}{2}\right|^2 \pm 2\left|\partial_s\langle x\rangle - m\frac{\langle x\rangle}{2}\right|\sqrt{\left|\partial_s\langle x\rangle - m\frac{\langle x\rangle}{2}\right|^2 + \frac{m^2}{4}}}\,. \tag{4.39}$$

Clearly, as $\langle x\rangle = 0$, it is $\widetilde{V}_+ = \widetilde{V}_- \equiv m/2$ as it should.[10] Also, the sum of the correlators above reads

$$C_{\text{sum}}(t)_{\langle x\rangle\neq 0} = \frac{(C_{\theta\theta}(t)_{\langle x\rangle\neq 0} + C_{\eta\eta}(t)_{\langle x\rangle\neq 0})}{2} \sim e^{-t\,\widetilde{V_-}} + e^{-t\,\widetilde{V_+}} \tag{4.40}$$

and thus justifies the choice for the fit functions in (4.36). We may also substitute in (4.39) the leading value for $\langle x\rangle$ obtained in perturbation theory in (B.10) (considering $\partial_s\langle x\rangle = 0$), thus obtaining for the exponential decay of the fermionic two-point functions above the expression

$$V_{\pm}^{\text{PT}} = \frac{m}{2}\frac{N\sqrt{2}}{g\,L\,m}\left(\sqrt{1 + \frac{(g\,L\,m)^2}{2\,N^2}} \pm 1\right). \tag{4.41}$$

Plotting the exponential decays $V_\pm$ obtained via MC measurements against $V_\pm^{\text{PT}}$ as in figure 6 one may notice a good convergence of the extrapolations to the expected values, at large g.

The observed divergence in the fermionic masses signals that the continuum limit should be redefined. In analogy with the case of chiral symmetry breaking of fermionic discretizations in lattice QCD (see e.g. [27]), one may interpret the divergence as an additive mass renormalisation of the bare coupling m and proceed by studying the violation of the continuum Ward identities on the lattice. We hope to report soon on this.

4.2 Impact of reweighting on observables

As explained in section 4, we perform simulations with a fermionic operator (4.1) modified both via the replacement (2.2) with the absolute value of its Pfaffian and by a small twisted-mass term to avoid the instabilities due to its near-zero modes. The sign of the Pfaffian and the low modes of O_F are then taken into account respectively by the reweighting W_s and W_μ in (4.3). Here we comment on the impact of such reweighting on the observables.

A pictorial way to study these effects is to look at the individual MC histories[11] of observables and reweighting factors, as well as the MC histories of their product (so, look at the observables "before" and "after" the reweighting). Figure 7 shows the MC evolution of the reweighting factors and of the observables as the simulation evolves, for two different values of the coupling $g = 5$ (left) and $g = 2$ (right) and the same value of the twisted-mass

[10] It is worth emphasizing that the continuum theory has full $\text{SO}(6)\times\text{U}(1)$ symmetry, in particular $\langle x\rangle = 0$. Namely, equations (4.37), (4.38) are written for illustrative purposes, supporting the interpretation that the divergence of the fermionic masses originates from symmetry breaking.

[11] In MC simulations, vacuum expectation values are replaced by ensemble averages. Ensembles are generated by a Markov process (here, the RHMC) and the MC history is the change of the observable along the Markov process. In this sense it only makes sense to compare MC histories from the same simulation (see e.g. [27]).

JHEP01(2020)174

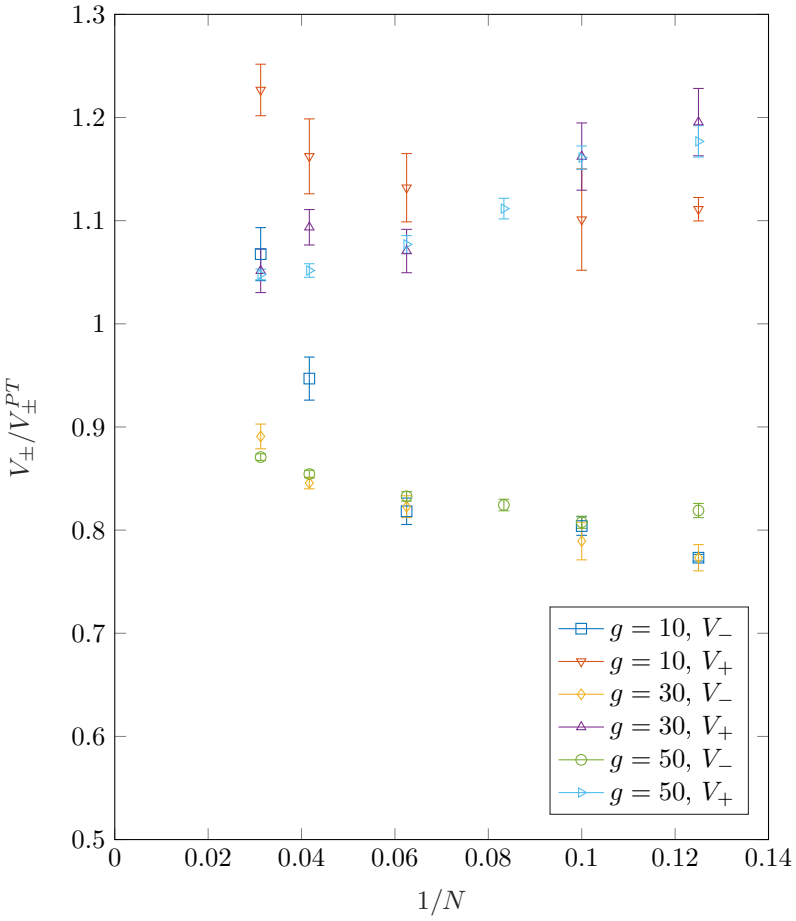

Figure 6. The ratio of the exponential decays obtained from the MC measurements (via the fit (4.36)) and and the PT prediction (4.41) for $g = 10, 30, 50$ and various values of N.

parameter $\mu = 0.01$. There appear to be no (statistical) correlation between the sign-reweighting W_s and the observables, nor between W_s and the μ-reweighting W_μ. However, as discussed in the previous section, small eigenvalues (and thus zero-crossings) are more probable to occur at lower g, which obviously reflects in a more severe sign problem (right diagram, $g = 2$).

As expected for bosonic observables, the fluctuations of the bosonic correlator are little correlated to those of the μ-reweighting factor W_μ. This is not so for the fermionic correlator. It is easy to spot a simultaneous occurrence of the negative peaks for the μ-reweighting for $g = 2$, upper right-diagram in figure 7, and the valleys in the value of the fermionic correlator (near MDU 20, 40 and 46).

This correspondence between W_μ and the fermionic correlator is due to the sensitivity of the two-point function, built out of the inverse fermionic operator, on the small eigenvalues of such operator, to which W_μ is also (by definition) sensitive.

In general, for the reweighting to work in practice, the fluctuations of the reweighting factor should be reasonably small (not to dominate the statistical error of the measured observable) [26, 36, 37]. Such fluctuations clearly depend on the choice of μ. A finite value

JHEP01(2020)174

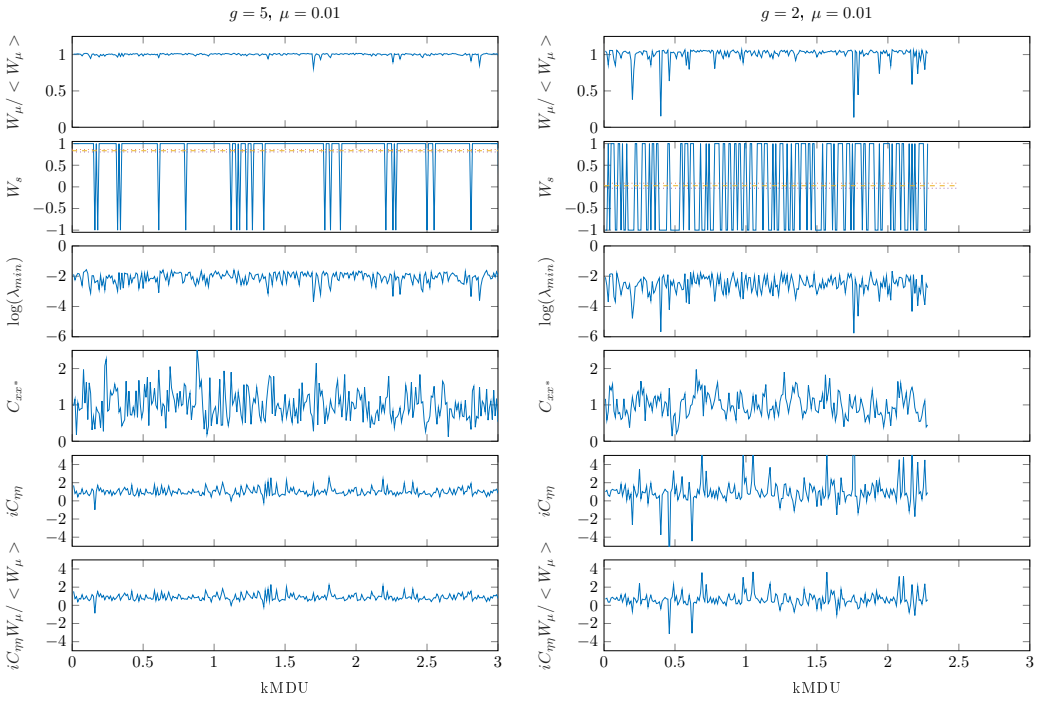

Figure 7. Time history of the reweighting factors W_μ and W_s in (4.3), the bosonic correlator $C_{xx}(t)$ and the fermionic correlator $C_{\eta\eta}(t)$ on two ensembles with $L = 8$, $\mu = 0.01$ and $g = 5$ (left), $g = 2$ (right). The correlators are evaluated on a time-slice $t = T/4$. The last three lines are normalized, so that they average to 1 (e.g. the third line is actually $C_{xx}/\langle C_{xx}\rangle$). For $g = 2$ there is a clear "correlation" between spikes in W_μ and the fermionic correlator.

of μ increases the ergodicity of the algorithm: field configurations with small eigenvalues of the original operator become statistically more significant in the path integral. On the other side, if μ becomes too large, the MC histories of fermionic correlators, which are controlled by the inverse of the modified operator, tend to develop sudden fluctuations. These fluctuations are unphysical, however they are cancelled in the ensemble average (4.2) by a smaller W_μ.

That the choice of μ should be made with care is clear from figure 8, where Monte Carlo histories are shown for two different values, $\mu = 0.01$ (left) and $\mu = 0.02$ (right), of the twisted-mass parameter and the same value $g = 5$ of the coupling. A doubled value of μ enhances of a factor of 10 the fluctuations of the reweighting factor W_μ (first line). The sign-reweighting W_s (second line, in which the red dotted lines represent the average) also appears to be sensitive to the fact that zero eigenvalues are more accessible for larger μ, something visible in the third line, where the logarithm of the lowest eigenvalue in the spectrum of $O_F O_F^\dagger$ appears. The bosonic correlator (fourth line) is as expected independent on the choice of the twisted-mass regulator. The situation is different for the fermionic correlator, which for larger μ develops spikes (fifth line). The spikes are cancelled, as expected, after reweighting (sixth line).

JHEP01(2020)174

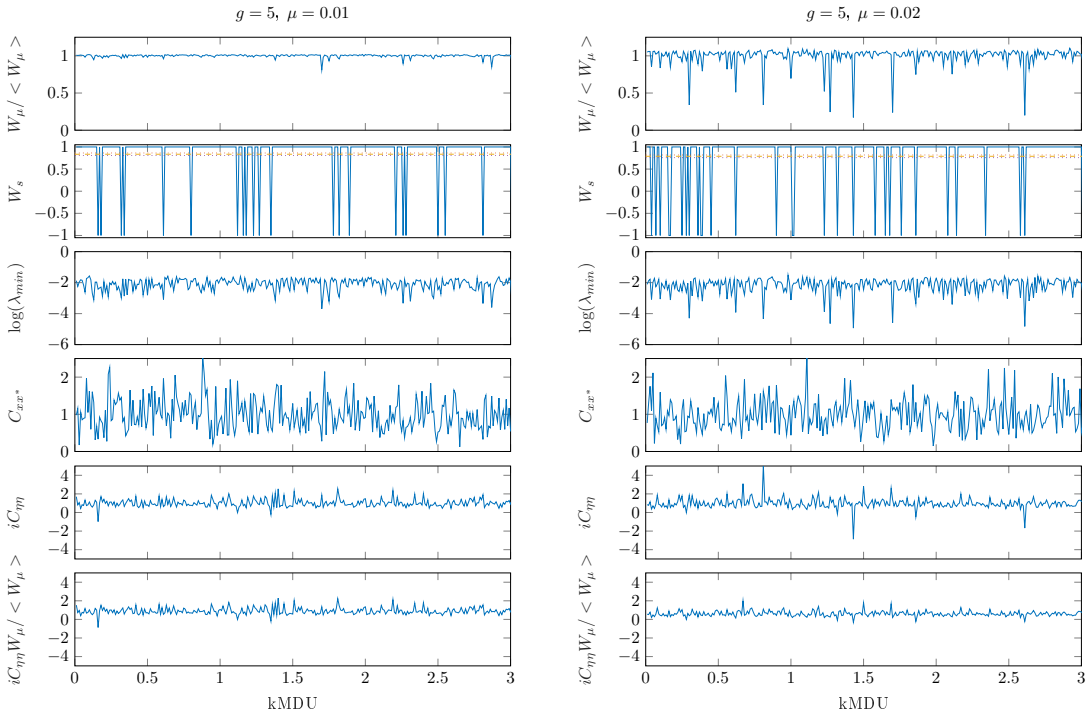

Figure 8. Time history of the reweighting factors W_μ and W_s in (4.3), the bosonic correlator $C_{xx}(t)$ and the fermionic correlator $C_{\eta\eta}(t)$ on two ensembles with $L = 8$, $g = 5$ with two different values of the reweighting parameter, $\mu = 0.01$ (left) and $\mu = 0.02$ (right). The correlators are evaluated on a time-slice $t = T/4$. The last three lines are normalized, so that they average to 1 (e.g. the third line is actually $C_{xx}/\langle C_{xx}\rangle$). For larger μ, zero eigenvalues are more accessible and the fermionic correlator develops spikes. The latter are cancelled after reweighting (sixth line).

A more quantitative way to see the effect of reweighting on the observables is a study of the covariance between the observables $\mathcal{O}$ and the reweighting factors W.[12] While we have observed that, as expected, the largest covariance is between the μ-reweighting and the value of the lowest eigenvalue of the fermionic operator, we could not in general draw a conclusive picture from this study because the effects are smaller than the statistical error.

Table 2 shows the effect of reweighting on the numerical values of the ensemble averages at one value of the coupling ($g = 5$) and two values $\mu = 0.01, 0.02$ of the μ-reweighting. It is interesting to notice that the sign-reweighting seems practically not to have effect on the measured observables. About the μ-reweighting, although not statistically significant, the effect is larger for the fermionic correlator.

Our last observation is about the behavior of the reweighting factors with the lattice spacing. This is done in figure 9. The sign-reweighting W_s shows a moderate (linear) dependence and tends towards zero for $1/N \to 0$. However, in the region of our simulations it is well above zero. The fluctuations of the μ-reweighting (at fixed μ) are small and compatible with an exponential dependence on N. Extrapolating these points simulations up to $N \sim 32$ seems feasible at $g = 5$.

[12] In particular, a vanishing covariance (from which $\langle \mathcal{O}\, W\rangle = \langle \mathcal{O}\rangle \langle W\rangle$) would imply the cancellation of $\langle W\rangle$ in (4.2). In this case the reweighting would not change the value of the observable, but only its variance.

JHEP01(2020)174

	$g=5,\ \mu=0.01$	$g=5,\ \mu=0.02$
$< C_{xx^*} >$	0.1620(44)	0.1619(31)
$< C_{xx^*} >_{W_s}$	0.1620(44)	0.1624(31)
$< C_{xx^*} >_{W}$	0.1604(49)	0.1643(38)
$< C_{\eta\eta^*} >$	0.1464(32)	0.1502(40)
$< C_{\eta\eta^*} >_{W_s}$	0.1461(32)	0.1505(34)
$< C_{\eta\eta^*} >_{W}$	0.1508(37)	0.1584(42)

Table 2. Effect of the reweighting on the two-point functions.

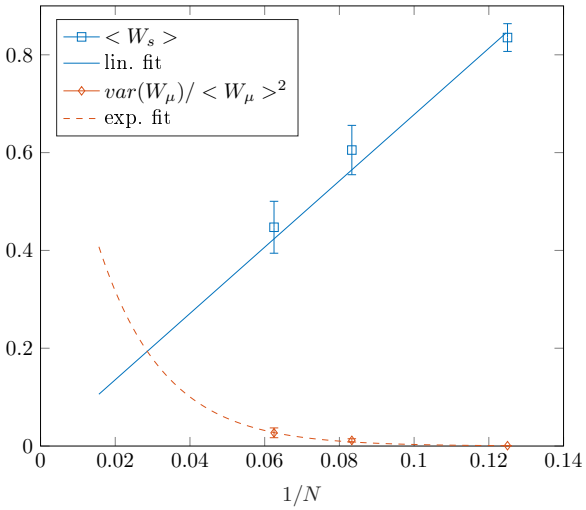

Figure 9. Lattice spacing dependence of $< W_s >$ and variance of W_μ at $g = 5$ and $\mu = 0.01$.

Acknowledgments

We are particularly grateful to Radu Roiban for several discussions. We thank Luigi Del Debbio, Michele Della Morte, Agostino Patella, Rainer Sommer and the members of the Innovative Training Network EuroPLEx for discussions. The research of LB received funding from the European Union's Horizon 2020 research and innovation programme under the Marie Sklodowska-Curie grant agreement No 749909. The research of VF received funding from the STFC grant ST/S005803/1, from the Einstein Foundation Berlin through an Einstein Junior Fellowship, and was supported in part by Perimeter Institute for Theoretical Physics and the Simons Foundation through a Simons Emmy Noether Fellowship. The research of EV received funding by the FAPESP grants 2014/18634-9 and 2016/09266-1, and by the STFC grant ST/P000762/1.

A Conventions and matrix algebra

In the action (2.1) we used the six 4×4 matrices $(\rho^M)_{ij}$, off-diagonal blocks of the SO(6), 8×8 Dirac matrices in chiral representation

$$\gamma^M \equiv \begin{pmatrix} 0 & \rho^\dagger_M \\ \rho^M & 0 \end{pmatrix} = \begin{pmatrix} 0 & (\rho^M)^{ij} \\ (\rho^M)_{ij} & 0 \end{pmatrix} \tag{A.1}$$

JHEP01(2020)174

for which

$$\rho^M_{ij} = -\rho^M_{ji}\,, \qquad (\rho^M)^{il}\rho^N_{lj} + (\rho^N)^{il}\rho^M_{lj} = 2\delta^{MN}\delta^i_j\,, \qquad (\rho^M)^{ij} \equiv -(\rho^M_{ij})^*\,. \tag{A.2}$$

A possible explicit representation is

$$\rho^1_{ij} = \begin{pmatrix} 0 & 1 & 0 & 0 \\ -1 & 0 & 0 & 0 \\ 0 & 0 & 0 & 1 \\ 0 & 0 & -1 & 0 \end{pmatrix}, \qquad \rho^2_{ij} = \begin{pmatrix} 0 & \mathrm{i} & 0 & 0 \\ -\mathrm{i} & 0 & 0 & 0 \\ 0 & 0 & 0 & -\mathrm{i} \\ 0 & 0 & \mathrm{i} & 0 \end{pmatrix}, \qquad \rho^3_{ij} = \begin{pmatrix} 0 & 0 & 0 & 1 \\ 0 & 0 & 1 & 0 \\ 0 & -1 & 0 & 0 \\ -1 & 0 & 0 & 0 \end{pmatrix},$$

$$\rho^4_{ij} = \begin{pmatrix} 0 & 0 & 0 & -\mathrm{i} \\ 0 & 0 & \mathrm{i} & 0 \\ 0 & -\mathrm{i} & 0 & 0 \\ \mathrm{i} & 0 & 0 & 0 \end{pmatrix}, \qquad \rho^5_{ij} = \begin{pmatrix} 0 & 0 & \mathrm{i} & 0 \\ 0 & 0 & 0 & \mathrm{i} \\ -\mathrm{i} & 0 & 0 & 0 \\ 0 & -\mathrm{i} & 0 & 0 \end{pmatrix}, \qquad \rho^6_{ij} = \begin{pmatrix} 0 & 0 & 1 & 0 \\ 0 & 0 & 0 & -1 \\ -1 & 0 & 0 & 0 \\ 0 & 1 & 0 & 0 \end{pmatrix}.$$

The SO(6) generators are built out of the ρ-matrices via

$$\rho^{MN\,i}{}_j \equiv \frac{1}{2}[(\rho^M)^{il}\rho^N_{lj} - (\rho^N)^{il}\rho^M_{lj}] \tag{A.3}$$

and the following identities hold

$$(\rho^{MN})^i{}_j = \left((\rho^{MN})_i{}^j\right)^* \qquad\qquad (\rho^{MN})^i{}_j = -(\rho^{MN})_j{}^i\,, \tag{A.4}$$

where in the last equation we used that $\frac{1}{2}(\rho^{M\,i\ell}\,\rho^N_{\ell j} - \rho^{N\,i\ell}\,\rho^M_{\ell j}) = -\frac{1}{2}(\rho^M_{j\ell}\,\rho^{N\,\ell i} - \rho^N_{j\ell}\,\rho^{M\,\ell i})$. Useful flipping rules are

$$\eta\,\rho^M\,\theta = \eta^i\,\rho^M_{ij}\,\theta^j = -\theta^j\,\rho^M_{ij}\,\eta^i = \theta^j\,\rho^M_{ji}\,\eta^i \equiv \theta^i\,\rho^M_{ij}\,\eta^j = \theta\,\rho^M\,\eta \tag{A.5}$$

$$\eta^\dagger\rho^\dagger_M\,\theta^\dagger = \eta_i\,\rho^{M\,ij}\,\theta_j = -\theta_j\,\rho^{M\,ij}\,\eta_i = \theta_j\,\rho^{M\,ji}\,\eta_i \equiv \theta_i\,\rho^{M\,ij}\,\eta_j = \theta^\dagger\rho^\dagger_M\,\eta^\dagger \tag{A.6}$$

$$\eta_i\,(\rho^{MN})^i{}_j\,\theta^j = -\theta^j\,(\rho^{MN})^i{}_j\,\eta_i = \theta^j\,(\rho^{MN})_j{}^i\,\eta_i \equiv \theta^i\,(\rho^{MN})_i{}^j\,\eta_j\,. \tag{A.7}$$

In the main text, for the steps leading from (2.3) to (2.5) we used the following additional properties

$$(\rho^M)^{im}(\rho^M)^{kn} = 2\epsilon^{imkn} \tag{A.8}$$

$$(\rho^M)^{im}(\rho^M)_{nj} = 2\left(\delta^i_j\delta^m_n - \delta^i_n\delta^m_j\right) \tag{A.9}$$

$$\begin{aligned}\epsilon^{imkn}(\rho^M)_{mj}(\rho^L)_{nl} + \epsilon_{mjnl}(\rho^M)^{im}(\rho^L)^{kn} &= (\rho^{\{M})^{ik}(\rho^{L\}})^{jl} \\ &\quad + \delta^k_j(\rho^L)^{im}(\rho^M)_{ml} + \delta^i_l(\rho^M)^{km}(\rho^L)_{mj} \\ &\quad + \delta^{ML}\left(-4\delta^i_l\delta^k_j + 2\delta^i_j\delta^k_l\right)\end{aligned} \tag{A.10}$$

$$-(\rho^{MN})^i{}_j(\rho^{ML})^k{}_l n_N n_L = -2(\rho^N)^{ik}(\rho^L)_{jl}n_N n_L - \delta^i_j\delta^k_l + 2\delta^i_l\delta^k_j \tag{A.11}$$

leading to the identification

$$\left(i\,\eta_i(\rho^{MN})^i{}_j n^N \eta^j\right)^2 = -3(\eta^2)^2 + 2\eta_i(\rho^N)^{ik}n_N\eta_k\eta^j(\rho^L)_{jl}n_L\eta^l \tag{A.12}$$

JHEP01(2020)174

Around equation (2.6) we also defined

$$\Sigma_i^j = \eta_i \eta^j \qquad \tilde{\Sigma}_j^i = (\rho^N)^{ik} n_N (\rho^L)_{jl} n_L \eta_k \eta^l \tag{A.13}$$

where we simply indicate $\Sigma_j^i = \Sigma^i{}_j = \Sigma_j{}^i$ since

$$\Sigma^i{}_j \equiv (\Sigma_i{}^j)^* = (\eta^j)^* (\eta_i)^* = \eta_j \eta^i = \Sigma_j{}^i \tag{A.14}$$

and similarly for $\tilde{\Sigma}$. It is simple to check that

$$\Sigma_i^j \Sigma_j^i = -(\eta^2)^2 \qquad \tilde{\Sigma}_i^j \tilde{\Sigma}_j^i = -(\eta^2)^2 \qquad \Sigma_j^i \tilde{\Sigma}_i^j = -\left|\eta_i (\rho^N)^{ik} n_N \eta_k\right|^2 \tag{A.15}$$

$$(\Sigma_i^j)^* = \Sigma_j^i \qquad (\tilde{\Sigma}_i^j)^* = \tilde{\Sigma}_j^i \tag{A.16}$$

We conclude this section with a detailed counting of the degrees of freedom implied in the Hubbard Stratonovich transformation (2.11). The 4×4 matrix Σ_+ is hermitian and contains 16 real d.o.f. One can project the two indices i and j onto irreducible $su(4)$ representations

$$\mathbf{4} \otimes \bar{\mathbf{4}} = \mathbf{15} \oplus \mathbf{1} \tag{A.17}$$

or, more explicitly

$$\Sigma_+{}_i^j = \frac{1}{4} (\rho^{MN})^j{}_i S_{MN} + \frac{1}{2} \delta_i^j S \tag{A.18}$$

The term $\mathrm{Tr}\Sigma_+\Sigma_+$ in the Lagrangian would read

$$\mathrm{Tr}\Sigma_+\Sigma_+ = \frac{1}{2} S_{MN} S^{MN} + S^2 \tag{A.19}$$

This is a sum of $15 + 1$ real terms (remember S_{MN} is an antisymmetric 6×6 matrix). To any of these terms one can associate, via a Hubbard Stratonovich transformation, a real scalar field (therefore 15 scalars ϕ_{MN} in the adjoint and one in the singlet). Then, by the opposite procedure one can rebuild the matrix ϕ_i^j used in (2.11). This proves that the matrix ϕ_i^j is hermitian.

B One-point function for x, x^*

In the continuum, the action (2.1) and its linearized version (2.12), (2.13), (2.14) enjoy the $\mathrm{SO}(6) \times \mathrm{U}(1)$ symmetry of the cusp background. In particular, the U(1) invariance implies $\langle x \rangle = \langle x^* \rangle = 0$. The Wilson-like discretization (2.15)–(2.17) adopted in this paper for the fermionic sector breaks the U(1) symmetry, and as a consequence the fields x, x^* acquire then a non-trivial, in fact divergent, 1-point function. We evaluate here this one-point function at leading order, $\mathcal{O}(g^{-1})$, in lattice perturbation theory.

The continuum sigma-model loop expansion for this model (in AdS light-cone gauge) is studied in [23, 24], and a first calculation in lattice perturbation theory appears in section 3 (see also appendix A) of [12]. Here we recall that in order to perform a perturbative computation, in the continuum and on the lattice, one cannot simply expand around the trivial vacuum where all the fields are set to zero — this is prevented by the presence of

JHEP01(2020)174

inverse powers of the radial coordinate z in the Lagrangian. One proceeds then picking one of the degenerate "null cusp" vacua corresponding to the SO(6) directions of z^M (this breaks the SO(6) symmetry to a SO(5)), say $u^M = (0,\,0,\,0,\,0,\,0,\,1)$, where u^M, with $u^M u^M = 1$ are part of the standard definition of Poincare' patch coordinates $\tilde{z}^M = e^{\tilde{\phi}}\tilde{u}^M$, $\tilde{z} = e^{\tilde{\phi}}$. In terms of

$$\tilde{u}^a = \frac{y^a}{1+\frac{1}{4}y^2}\,, \qquad \tilde{u}^6 = \frac{1-\frac{1}{4}y^2}{1+\frac{1}{4}y^2}\,, \qquad\qquad y^2 \equiv \sum_{a=1}^{5}(y^a)^2\,, \qquad a=1,\ldots,5\,, \tag{B.1}$$

the vacuum corresponds then to $y^a = \phi = 0$.

Because of our Wilson discretization, the diagonal fermionic propagators $C_{\eta^i\eta^i}$ and $C_{\eta_i\eta_i}$, corresponding to the two lower diagonal entries of (4.20), are non-vanishing. The cubic interaction

$$S_{x\eta\eta} = 2g\int dt\,ds\left[\eta^i\,\rho^M_{ij}\,\eta^j\left(\partial_s x - \frac{m}{2}x\right)u^M - \eta_i\,\rho^{ij}_M\,\eta_j\left(\partial_s x^* - \frac{m}{2}x^*\right)u^m\right], \tag{B.2}$$

gives then a contribution at order $1/g$ to the 1-point function of x, x^* through a tadpole graph with a single fermionic loop. In momentum space the relevant propagators read

$$C_{xx^*}(p_0,p_1) = \frac{1}{g}\frac{2}{\hat{p}^2+\frac{m^2}{2}} \tag{B.3}$$

$$C_{\eta_i\eta_j}(p_0,q_1) = \frac{a}{g}\,[K_F^{-1}(p_0,p_1)]_{44} = -\frac{a\,r}{2\,g}\frac{(\hat{p}_0^2 - i\,\hat{p}_1^2)\,\rho^M_{ij}u^M}{[\det K_F(p_0,p_1)]^{1/8}} \tag{B.4}$$

$$C_{\eta^i\eta^j}(p_0,q_1) = \frac{a}{g}\,[K_F^{-1}(p_0,p_1)]_{33} = \frac{a\,r}{2\,g}\frac{(\hat{p}_0^2 + i\,\hat{p}_1^2)\,\rho^{ij}_M u^M}{[\det K_F(p_0,p_1)]^{1/8}}\,. \tag{B.5}$$

where the bosonic one (B.3) is obtained from the continuum [12, 23] with the naive replacement $p_\mu \to \hat{p}_\mu$, and the fermionic propagators are taken from (4.20)–(4.21)–(4.22).

For the x-field, Wick-contracting and using (B.3) and (B.4) and the second term in (B.2), one writes formally, in momentum space, at leading order (LO) in $1/g$ expansion

$$\begin{aligned}\langle\tilde{x}(q)\rangle_{\rm LO} = \frac{8\,r\,a}{g}\,\delta^{(2)}(q)\,\frac{i\,\hat{q}_1 - \frac{m}{2}}{\hat{q}^2+\frac{m^2}{2}}\,u^M\rho^{ij}_M\rho^N_{ij}u^N \\ \times\iint_{-\frac{\pi}{a}}^{\frac{\pi}{a}}\frac{d^2p}{(2\pi)^2}\,\frac{\hat{p}_0^2 - i\,\hat{p}_1^2}{\mathring{p_0}^2+\mathring{p_1}^2+\frac{m^2}{4}+\frac{a^2\,r^2}{4}\left(\hat{p}_0^4+\hat{p}_1^4\right)}\,,\end{aligned} \tag{B.6}$$

where we denoted with q the 2-momentum of the external bosonic field x, with p_0, p_1 the 2-momentum of the fermion in the loop and we used (4.21). Above, $\delta^{(2)}(q)$ is the momentum conservation at the vertex. Rescaling the momenta with the lattice spacing, using that (A.2) implies $\rho^{ij}_M\rho^N_{ij}u^M u^N = -4$ and setting $r=1$ one obtains

$$\langle\tilde{x}(q)\rangle_{\rm LO} = -\frac{32}{g\,a}\,(1-i)\,I(M)\,\delta^{(2)}(q)\frac{i\,\hat{q}_1 - \frac{m}{2}}{\hat{q}^2+\frac{m^2}{2}}\,, \tag{B.7}$$

where $(M = m\,a)$

$$I(M) = \int_{-\pi}^{\pi}\frac{dp_0\,dp_1}{(2\pi)^2}\,\frac{\sin^2\frac{p_0}{2}}{\sin^2 p_0 + \sin^2 p_1 + 4\sin^4\frac{p_0}{2} + 4\sin^4\frac{p_1}{2} + M^2}\,, \quad \text{with} \quad I(0) = \frac{1}{32}\,. \tag{B.8}$$

JHEP01(2020)174

Fourier transforming back in position space one obtaines

$$\begin{aligned}\langle x\rangle_{\rm LO} &= \iint_{-\frac{\pi}{a}}^{\frac{\pi}{a}} dq_0 dq_1\, e^{-it\,q_0 - is\,q_1}\,\langle \tilde{x}(q)\rangle \\ &= -\frac{32}{g\,a}\,(1-i)\,I(M)\iint_{-\frac{\pi}{a}}^{\frac{\pi}{a}} dq_0 dq_1\,\delta(q_0)\,\delta(q_1)\,e^{-it\,q_0 - is\,q_1}\,\frac{\frac{i}{a}\,\sin\frac{q_1}{2} - \frac{m}{2}}{\frac{1}{a^2}\sin^2\frac{q_0}{2} + \frac{1}{a^2}\sin^2\frac{q_1}{2} + \frac{m^2}{2}} \\ &= -\frac{32}{g}\,(1-i)\,I(M)\,\frac{1}{m\,a}\ .\end{aligned} \tag{B.9}$$

Using that in the continuum limit $a \to 0$ the product $m\,L = M\,N$ is fixed and that $I(0) = \frac{1}{32}$, we find that the one-point function diverges linearly in N $(= L/a)$ as

$$\langle x\rangle_{\rm LO} = \frac{N}{g\,m\,L}(1-i)\,. \tag{B.10}$$

This result is perfectly consistent with the plot of figure 3 for several values of (large) g. Repeating the computation for the field x^*, therefore using the first term in (B.2) and (B.4), it is easy to verify that

$$\langle x^*\rangle_{\rm LO} = \frac{N}{g\,m\,L}(1+i)\,. \tag{B.11}$$

The two equations above are consistent with (4.12) at leading $(1/g)$ order in sigma-model perturbation theory.

Open Access. This article is distributed under the terms of the Creative Commons Attribution License (CC-BY 4.0), which permits any use, distribution and reproduction in any medium, provided the original author(s) and source are credited.

References

[1] S. Catterall, D.B. Kaplan and M. Ünsal, *Exact lattice supersymmetry*, *Phys. Rept.* **484** (2009) 71 [arXiv:0903.4881] [INSPIRE].

[2] D. Schaich, *Aspects of lattice $\mathcal{N} =$ supersymmetric Yang-Mills*, PoS(LATTICE 2015)242 [arXiv:1512.01137] [INSPIRE].

[3] A. Joseph, *Review of lattice supersymmetry and gauge-gravity duality*, *Int. J. Mod. Phys.* **A 30** (2015) 1530054 [arXiv:1509.01440] [INSPIRE].

[4] G. Bergner and S. Catterall, *Supersymmetry on the lattice*, *Int. J. Mod. Phys.* **A 31** (2016) 1643005 [arXiv:1603.04478] [INSPIRE].

[5] D. Schaich, S. Catterall, P.H. Damgaard and J. Giedt, *Latest results from lattice $N = 4$ supersymmetric Yang-Mills*, PoS(LATTICE2016)221 [arXiv:1611.06561] [INSPIRE].

[6] E. Berkowitz et al., *Precision lattice test of the gauge/gravity duality at large-N*, *Phys. Rev.* **D 94** (2016) 094501 [arXiv:1606.04951] [INSPIRE].

[7] E. Rinaldi et al., *Toward holographic reconstruction of bulk geometry from lattice simulations*, *JHEP* **02** (2018) 042 [arXiv:1709.01932] [INSPIRE].

JHEP01(2020)174

[8] S. Catterall, R.G. Jha, D. Schaich and T. Wiseman, *Testing holography using lattice super-Yang-Mills theory on a 2-torus*, *Phys. Rev.* **D 97** (2018) 086020 [arXiv:1709.07025] [INSPIRE].

[9] D. Schaich, *Progress and prospects of lattice supersymmetry*, PoS(LATTICE2018)005 [arXiv:1810.09282] [INSPIRE].

[10] R.W. McKeown and R. Roiban, *The quantum $AdS_5 \times S^5$ superstring at finite coupling*, arXiv:1308.4875 [INSPIRE].

[11] V. Forini et al., *Lattice and string worldsheet in AdS/CFT: a numerical study*, PoS(LATTICE 2015)244 [arXiv:1601.04670] [INSPIRE].

[12] L. Bianchi et al., *Green-Schwarz superstring on the lattice*, *JHEP* **07** (2016) 014 [arXiv:1605.01726] [INSPIRE].

[13] V. Forini et al., *Strings on the lattice and AdS/CFT*, PoS(LATTICE2016)206 [arXiv:1702.02005] [INSPIRE].

[14] V. Forini, *On regulating the AdS superstring*, pp. 221–244, (2018), arXiv:1712.10301, DOI [INSPIRE].

[15] N. Beisert, B. Eden and M. Staudacher, *Transcendentality and crossing*, *J. Stat. Mech.* **0701** (2007) P01021 [hep-th/0610251] [INSPIRE].

[16] B. Basso, A. Sever and P. Vieira, *Spacetime and flux tube S-matrices at finite coupling for $N = 4$ supersymmetric Yang-Mills theory*, *Phys. Rev. Lett.* **111** (2013) 091602 [arXiv:1303.1396] [INSPIRE].

[17] B. Basso, A. Sever and P. Vieira, *Space-time S-matrix and flux tube S-matrix II. Extracting and matching data*, *JHEP* **01** (2014) 008 [arXiv:1306.2058] [INSPIRE].

[18] D. Fioravanti, S. Piscaglia and M. Rossi, *Asymptotic Bethe Ansatz on the GKP vacuum as a defect spin chain: scattering, particles and minimal area Wilson loops*, *Nucl. Phys.* **B 898** (2015) 301 [arXiv:1503.08795] [INSPIRE].

[19] A. Bonini, D. Fioravanti, S. Piscaglia and M. Rossi, *Fermions and scalars in $\mathcal{N} = 4$ Wilson loops at strong coupling and beyond*, *Nucl. Phys.* **B** (2019) 114644 [arXiv:1807.09743].

[20] R.R. Metsaev and A.A. Tseytlin, *Superstring action in $AdS_5 \times S^5$. Kappa symmetry light cone gauge*, *Phys. Rev.* **D 63** (2001) 046002 [hep-th/0007036] [INSPIRE].

[21] R.R. Metsaev, C.B. Thorn and A.A. Tseytlin, *Light cone superstring in AdS space-time*, *Nucl. Phys.* **B 596** (2001) 151 [hep-th/0009171] [INSPIRE].

[22] S.S. Gubser, I.R. Klebanov and A.M. Polyakov, *A semiclassical limit of the gauge/string correspondence*, *Nucl. Phys.* **B 636** (2002) 99 [hep-th/0204051] [INSPIRE].

[23] S. Giombi et al., *Quantum $AdS_5 \times S^5$ superstring in the AdS light-cone gauge*, *JHEP* **03** (2010) 003 [arXiv:0912.5105] [INSPIRE].

[24] S. Giombi, R. Ricci, R. Roiban and A.A. Tseytlin, *Quantum dispersion relations for excitations of long folded spinning superstring in $AdS_5 \times S^5$*, *JHEP* **01** (2011) 128 [arXiv:1011.2755] [INSPIRE].

[25] S. Giombi, R. Ricci, R. Roiban and A.A. Tseytlin, *Two-loop $AdS_5 \times S^5$ superstring: testing asymptotic Bethe ansatz and finite size corrections*, *J. Phys.* **A 44** (2011) 045402 [arXiv:1010.4594] [INSPIRE].

JHEP01(2020)174

[26] M. Lüscher and F. Palombi, *Fluctuations and reweighting of the quark determinant on large lattices*, PoS(LATTICE 2008)049 [arXiv:0810.0946] [INSPIRE].

[27] I. Montvay and G. Muenster, *Quantum fields on a lattice*, Cambridge University Press, Cambridge U.K. (1994).

[28] S. Catterall, *Fermion mass without symmetry breaking*, *JHEP* **01** (2016) 121 [arXiv:1510.04153] [INSPIRE].

[29] S. Catterall and D. Schaich, *Novel phases in strongly coupled four-fermion theories*, *Phys. Rev.* **D 96** (2017) 034506 [arXiv:1609.08541] [INSPIRE].

[30] J. Finkenrath, F. Knechtli and B. Leder, *One flavor mass reweighting in lattice QCD*, *Nucl. Phys.* **B 877** (2013) 441 [*Erratum ibid.* **B 880** (2014) 574] [arXiv:1306.3962] [INSPIRE].

[31] M. Wimmer, *Algorithm 923: efficient numerical computation of the Pfaffian for dense and banded skew-symmetric matrices*, *ACM Trans. Math. Soft.* **38** (2012) 30.

[32] ALPHA collaboration, *Monte Carlo errors with less errors*, *Comput. Phys. Commun.* **156** (2004) 143 [*Erratum ibid.* **176** (2007) 383] [hep-lat/0306017] [INSPIRE].

[33] A.D. Kennedy, I. Horvath and S. Sint, *A new exact method for dynamical fermion computations with nonlocal actions*, *Nucl. Phys. Proc. Suppl.* **73** (1999) 834 [hep-lat/9809092] [INSPIRE].

[34] M.A. Clark and A.D. Kennedy, *The RHMC algorithm for two flavors of dynamical staggered fermions*, *Nucl. Phys. Proc. Suppl.* **129** (2004) 850 [hep-lat/0309084] [INSPIRE].

[35] B. Basso, *Exciting the GKP string at any coupling*, *Nucl. Phys.* **B 857** (2012) 254 [arXiv:1010.5237] [INSPIRE].

[36] M. Bruno et al., *On the extraction of spectral quantities with open boundary conditions*, PoS(LATTICE2014)089 [arXiv:1411.5207] [INSPIRE].

[37] M. Bruno et al., *Simulation of QCD with $N_f = 2 + 1$ flavors of non-perturbatively improved Wilson fermions*, *JHEP* **02** (2015) 043 [arXiv:1411.3982] [INSPIRE].

JHEP01(2020)174